Targeted ablation of Arnt in mouse epidermis results in profound defects in desquamation and epidermal barrier function

Songmei Geng[1,*,‡], Alexandre Mezentsev[1,‡], Sergey Kalachikov[2], Klaus Raith[3], Dennis R. Roop[4] and Andrey A. Panteleyev[1,§]

[1]Departmnet of Dermatology and [2]Columbia Genome Center, Columbia University, New York, NY, USA
[3]Institute of Pharmaceutics and Biopharmaceutics, Martin Luther University, Halle, Germany
[4]Departments of Molecular and Cellular Biology and Dermatology, Baylor College of Medicine, Houston, TX, USA

*Present address: Department of Dermatology, Second Hospital, Xi'an Jiaotong University, Xi'an, People's Republic of China
‡These authors contributed equally to this work
§Author for correspondence (e-mail: ap374@columbia.edu)

Accepted 27 September 2006
Journal of Cell Science 119, 4901-4912 Published by The Company of Biologists 2006
doi:10.1242/jcs.03282

Summary

The molecular mechanisms of skin adaptation to the environmental stress are poorly understood. The aryl hydrocarbon receptor nuclear translocator (Arnt) lies at the intersection of several crucial adaptive pathways. Nevertheless, its role in adaptation of the skin to environmental stress has just begun to be unraveled. Here we show that Arnt is expressed in human and mouse skin in a developmentally dependent manner. Targeted K14-driven deletion of *Arnt* in the mouse epidermis resulted in early postnatal death, associated with a failure of epidermal barrier function. Gene expression profiling of Arnt-null mouse epidermis revealed upregulation of genes of the epidermal differentiation complex on mouse chromosome 3, including S100a genes (S100a8, S100a9, S100a10) and genes coding for small proline-rich proteins (Sprr1a, Sprr2i, Sprr2j, Sprrl1). HPTLC analysis showed significant accumulation of Cer[NS] and Cer[NH] ceramide species in Arnt-null epidermis, suggesting alterations in lipid metabolism. Continuous retention of corneosomes in Arnt-null epidermis that resulted in an abnormally dense corny layer and impaired desquamation was associated with upregulation of *Slpi*, an inhibitor of stratum corneum chymotryptic enzyme (SCCE) that plays a key role in corneosome degradation. The functional defects in Arnt-null mouse epidermis underscore the crucial role of Arnt in the maintenance of epidermal homeostasis, especially during the perinatal transition to the ex utero environment.

Supplementary material available online at
http://jcs.biologists.org/cgi/content/full/119/23/4901/DC1

Key words: Corneosome, Ceramides, Epidermal differentiation complex, SCCE

Introduction

The Aryl hydrocarbon Receptor Nuclear Translocator (Arnt) is a member of the basic helix-loop-helix (bHLH)-Per-Arnt-Sim (PAS) family of proteins which serve as dimeric transcription factors (Reyes et al., 1992). The PAS domain is a region containing two direct repeats of 44 amino acids (Fig. 1C) that mediates the heterodimerization between various members of this family and transcriptional activity of the resulting dimers (reviewed by Schmidt and Bradfield, 1996). PAS proteins mediate diverse biological functions including sensing of light, gases (oxygen, carbon monoxide, nitric oxide), reactive oxygen species, redox potential, small toxic ligands and the overall energy level of the cell (Reyes et al., 1992; Taylor and Zhulin, 1999; Gu et al., 2000). Whereas most PAS proteins heterodimerize with a single partner, Arnt plays a unique role as a promiscuous heterodimerization partner within this family, thus falling squarely at the center of several crucial adaptive pathways.

The key role of Arnt in maintenance of homeostasis is supported by the early embryonic lethality of Arnt-null mice as a result of severe neural tissue malformations, cardiac dysfunction, abnormal hematopoiesis and failure of vasculogenesis (Kozak et al., 1997; Maltepe et al., 1997; Adelman et al., 1999). Previous studies in mouse embryos revealed high levels of Arnt expression in the brain, spinal cord, branchial arches, heart, primitive gut, hepatic primordium, otic and optic placodes, adrenal gland, tongue, bone, lung, testes and muscle (Jain et al., 1998). In late embryos, Arnt is also expressed in different epithelia, including skin (Aitola et al., 2003). In neonatal and adult laboratory animals, a high level of Arnt expression has been shown in the CNS (Huang et al., 2000) and reproductive organs (Hasan and Fisher, 2003). Although Arnt has pleiotropic functions, its role in transcriptional control has been defined in only two pathways: the toxic response to dioxin-like environmental pollutants and hypoxia (Schmidt and Bradfield, 1996).

Arnt was first identified as a factor essential for the response of mouse hepatoma cells to the environmental contaminant dioxin (2,3,7,8-tetrachlorodibenzo-*p*-dioxin) (Hoffman et al., 1991) and later, Arnt was found to be indispensable for the transcriptional activity of dioxin-specific Aryl-hydrocarbon receptor (Ahr) (reviewed by Schmidt and Bradfield, 1996;

Mimura and Fujii-Kuriyama, 2003). Ahr/Arnt heterodimers mediate various biological effects of dioxin such as teratogenesis, hepatotoxicity, tumorigenesis, epithelial dysplasia and immunosuppression (Poland and Knutson, 1982; Mimura and Fujii-Kuriyama, 2003). The target genes for the Ahr/Arnt heterodimer in mediating these effects of dioxin toxicity, as well as the endogenous ligand for Ahr, remain unknown.

The second Arnt-dependent pathway, hypoxia, is associated with numerous pathological conditions and is a critical regulator of cell proliferation, expansion and survival. Hypoxia-induced factor Hif-1, a key regulator of hypoxic

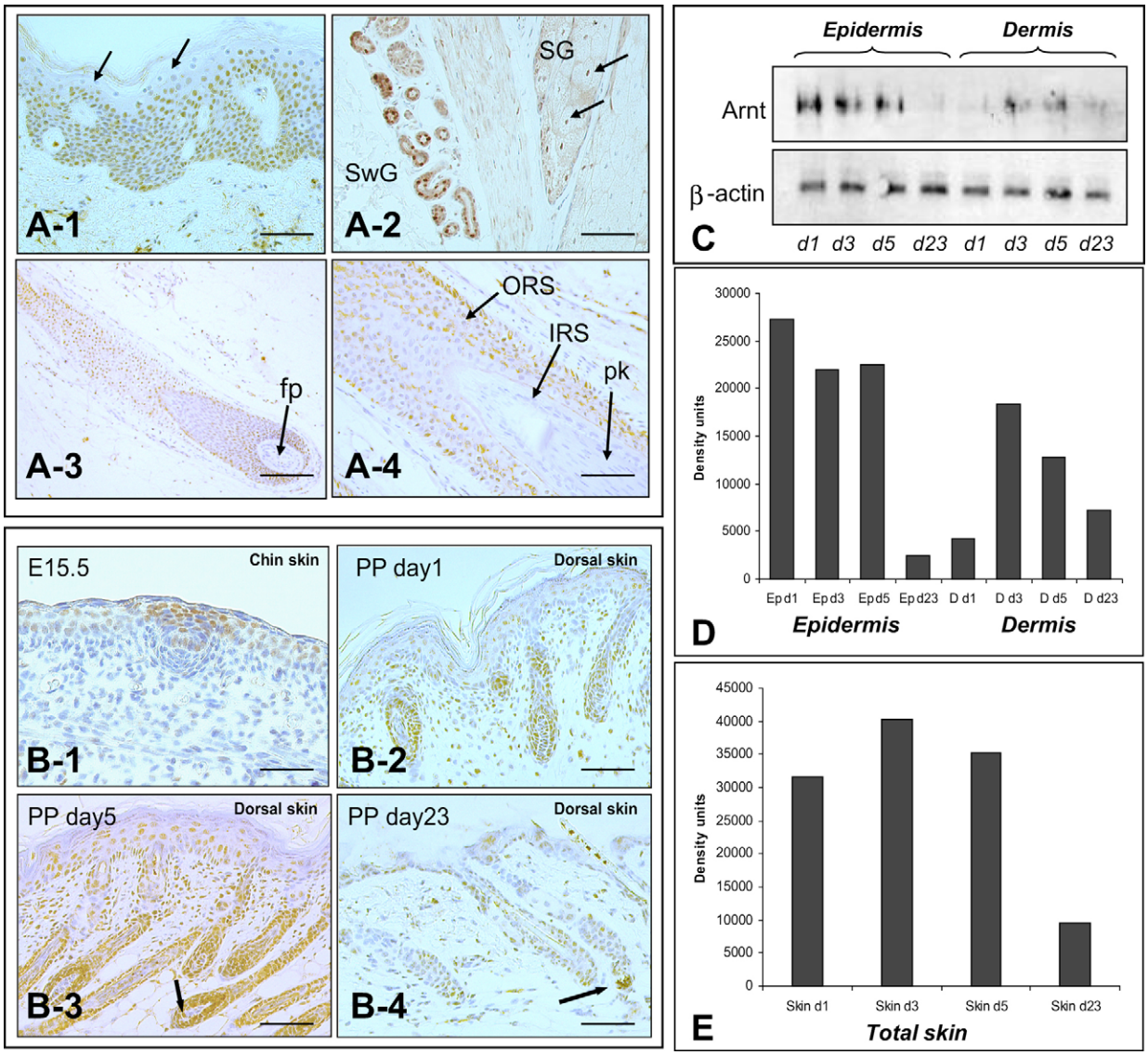

Fig. 1. Arnt immunohistochemistry in human (A) and mouse (B) skin. Deparaffinized skin sections were incubated with anti-Arnt antibodies and processed using the ABC procedure. (A-1) In normal human epidermis, Arnt-positive nuclei are seen in the basal and spinous layers whereas the granular layer (arrows) is mostly negative. (A-2) Intensive Arnt expression is seen in the nuclei of the sweat gland (SwG) epithelium and in the nuclei of cebocytes (arrows). (A-3) Follicular papilla (fp) fibroblasts are negative, whereas hair matrix cells are positive. (A-4) A close-up of the middle portion of a human hair follicle (HF) shows cells with positive nuclei in the outer root sheath (ORS), whereas the inner root sheath (IRS) and precortex cells (pk) are negative. (B-1) In embryonic mouse skin (E15.5), moderate Arnt expression is seen in the epidermis, concentrated above the hair placode. The mesenchymal compartment is negative. (B-2) During the initial stages of HF morphogenesis, the interfollicular epidermis shows low-to-moderate Arnt expression, whereas in growing HFs high expression is seen in the matrix and in the middle ORS. (B-3) With completion of HF morphogenesis, Arnt expression in both HF and epidermis significantly increases; dermal cells and follicular papilla fibroblasts are also positive. (B-4) In catagen-telogen, follicular papilla (FP) cells (arrows) are highly positive, whereas in the HF and the epidermis Arnt immunoreactivity declines and is seen mainly in the basal layer and HF ORS. (C) Western blot with protein samples isolated from dermis and epidermis at different stages of postnatal development of normal C57BL/6 mice (days 1-23 post partum). (D) Quantification of western blot data using a FluorChem 8800 digital image system showed gradual decline of Arnt expression in the mouse epidermis during the first days of life whereas in the dermis (including HFs) and in total skin (E) it increases between days 1 and 3 and then decreases. Bars, 40 μm (A-4, B-1); 60 μm (A-1, A-2, B-2, B-3, B-4); 120 μm (A-3).

response, is a heterodimer of two PAS proteins – Hif-1α and Arnt, which is also designated as the Hif-1β subunit (Adelman et al., 1999; Lee et al., 2004). The Arnt/Hif-1α heterodimer is a global regulator of hypoxia-specific gene expression and controls many responses to low oxygen including adaptation to anaerobic metabolism, erythropoiesis, angiogenesis, vasodilation, and possibly breathing (Guillemin and Krasnow, 1997; Gassmann et al., 1997; Gu et al., 2000; Goda et al., 2003).

The crucial role of Arnt in the toxic response to polyhalogenated compounds and in hypoxia-induced regulatory pathway upholds the designation of Arnt as a key regulator of adaptation to environmental insult (Gu et al., 2000).

The skin, as the protective shield of the body, possesses effective means of sensing and adapting to environmental factors. One of the most vital aspects of this protective mechanism is the epidermal barrier which is maintained by the uppermost layer of the epidermis – the stratum corneum. According to the current dogma, the stratum corneum is not simply a protective mechanical cover, but also a 'biosensor' that employs sophisticated mechanisms inducing proteolysis, DNA/lipid synthesis, and inflammation in response to the subtle changes of the environment (Elias et al., 2004). The pivotal role of Arnt in sensory pathways in brain, liver and reproductive organs (Gu et al., 2000; Xu et al., 2005; Hombach-Klonisch et al., 2005), as well as the striking skin symptoms in dioxin toxicity (Kuratsune, 1980; Crow, 1983; Poskitt et al., 1994; Geusau et al., 2000), led us to hypothesize that Arnt is a potential key element of skin-environment communication, yet the role of Arnt in skin functioning is just beginning to be unraveled (Takagi et al., 2003).

To better define the function of Arnt in maintenance of skin homeostasis, we first determined the temporo-spatial pattern of Arnt expression in mouse and human skin, and then developed an Arnt-deficient mouse model using K14-driven Cre-mediated recombination. Epidermal ablation of Arnt resulted in early postnatal death associated with multiple epidermal defects, including impairment of the epidermal barrier, cornified envelope formation, ceramide composition and corneosome degradation. These functional abnormalities were associated with profound molecular changes in the epidermis, including deregulation of serine protease inhibitors and the genes of the epidermal differentiation complex (EDC).

We propose, that in mammals, Arnt is not only involved in regulating toxic and hypoxia responses, but also serves as a crucial regulator of epidermal barrier function, especially during the perinatal transition to the terrestrial environment.

Results

Expression patterns of Arnt in mouse and human skin

Although a high level of Arnt expression was previously found in embryonic mouse skin and keratinocyte cell cultures (Jones and Reiners, Jr, 1997; Wanner et al., 1996), the patterns of Arnt expression in postnatal rodent and human skin were never assessed.

Using immunohistochemistry on normal human epidermis, Arnt was detected in the nuclei of the basal and most of the suprabasal keratinocytes, whereas the granular layer showed a lower level of Arnt expression (Fig. 1A-1). Strong expression of Arnt was also found in the hair follicle (HF) outer root sheath (ORS) and in the peripapillar cells of the hair matrix (Fig. 1A-3). It is of interest that the basal layer of the ORS in the lower (suprabulbar) follicle was negative, whereas in the middle and especially in the bulge-region the ORS basal cells showed strong nuclear Arnt staining. Intensive nuclear staining of Arnt was also seen in sebaceous and sweat glands (Fig. 1A-2). The HF inner root sheath, companion layer, precortex and hair shaft cells were negative (Fig. 1A-4) as well as the follicular papilla (FP) and most of the dermal fibroblasts (Fig. 1A-3).

In mouse skin at embryonic day 15.5 (E15.5), moderate expression of Arnt was seen in the epidermis with higher levels in the uppermost layers, and interestingly, a cluster of strongly Arnt-positive epidermal cells was seen just above the newly-formed hair placode (Fig. 1B-1). The mesenchymal components of the skin (dermis and dermal condensations) were mostly negative.

In the epidermis of newborn mice (postpartum day 1; P1), Arnt expression was detected in the spinous layer and in some basal cells (Fig. 1B-2). During the first week of life the level of Arnt expression in mouse epidermis remained high (Fig. 1B-3,C,D), nevertheless, during transformation of the epidermis from a thick multilayered 'neonatal' type with a prominent corny layer into a 'mature', thin structure (compare Fig. 1B-3 with Fig. 1B-4), which normally happens between P6 and P10, the expression of Arnt significantly declined (Fig. 1C,D) and changed from nearly ubiquitous (Fig. 1B-3) to spatially restricted, concentrating mostly in the basal cells (Fig. 1B-4).

In the growing mouse HFs, Arnt expression was high in the hair matrix and ORS similar to human HFs, but in contrast to human skin, Arnt was also present in most follicular papilla fibroblasts (Fig. 1B-2).

In the dermis, the intensity of Arnt expression gradually increased during the first days of postnatal development reaching its maximum by days 3-5 (Fig. 1B-3,C,D) and then it significantly declined (Fig. 1B-4,C,D).

By the third week after birth when HF morphogenesis was completed, Arnt expression gradually declined in both the epidermal and dermal (including HFs) components (Fig. 1D,E), with remaining Arnt positivity only observed in the basal layer of epidermis, ORS and follicular papilla cells (Fig. 1B-4).

Targeted ablation of Arnt in the epidermis of *Arnt*$^{flox/flox}$:K14Cre^{+} mice

Mice that lack functional Arnt do not survive after day 10.5 of embryonic development (Maltepe et al., 1997). In order to overcome the problem of embryonic lethality and develop a mouse model to study Arnt functions in skin, we attained spatially restricted *Arnt* gene inactivation by using keratin 14-driven Cre-mediated loxP recombination.

Pups lacking Arnt in the epidermis (*Arnt*$^{flox/flox}$:K14Cre^{+} or *Arnt*$^{\Delta/\Delta}$) because of homozygous Cre-mediated deletion of exon 6, which codes for the bHLH region of the *Arnt* gene (Fig. 2A-C), were born at the expected Mendelian ratio, indicating that ablation of Arnt activity in skin does not result in embryonic lethality. Western blots performed with proteins isolated from the epidermis of *Arnt*$^{\Delta/\Delta}$ newborns and cultured *Arnt*$^{\Delta/\Delta}$ keratinocytes showed a complete absence of Arnt

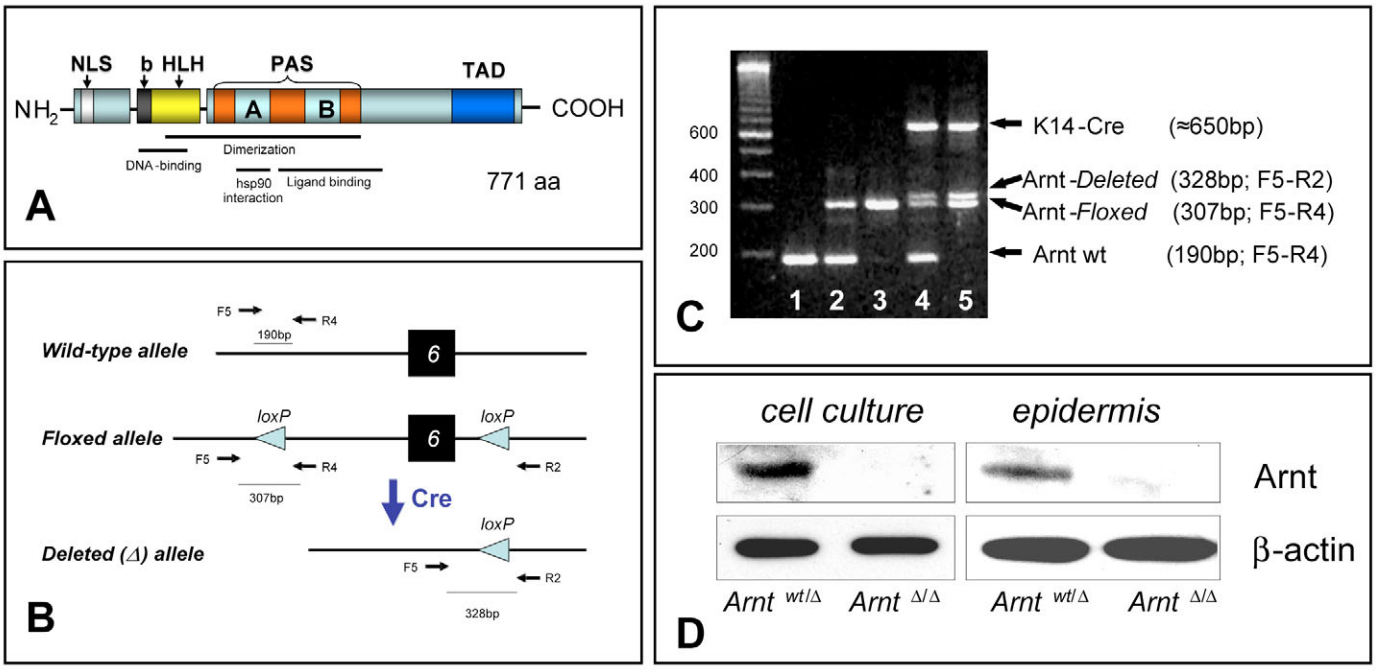

Fig. 2. Generation of Arnt-deficient mice. (A) Domain structure of Arnt. NLS, nuclear localization signal; bHLH, basic helix-loop-helix domain; PAS, Per-Arnt-Sim domain; TAD, transcription activation domain. (B) Generation of a K14-driven Arnt-deficient mouse model. LoxP sites flank exon 6 of the *Arnt* gene (see Tomita et al., 2000). Activity of Cre recombinase is introduced by crossbreeding of Arnt-floxed and K14-Cre animals, resulting in the excision of the exon 6 encoding the bHLH domain. (C) PCR analysis of the progeny obtained from crossbreeding of $Arnt^{flox/flox}$ and K14-Cre mice. Lane 1, Arnt wild-type allele; lane 2, $Arnt^{flox/-}$:K14-Cre^{-}; lane 3, $Arnt^{floxflox}$:14-Cre^{-}; lane 4, $Arnt^{flox/-}$:K14-Cre^{+}, deleted (Δ) band is present; lane 5, $Arnt^{flox/flox}$:K14-Cre^{+}, deleted (Δ) band is present. The presence of the undeleted (floxed) bands in lanes 4 and 5 is explained by contamination of the sample with genomic DNA from K14-negative tissues (e.g. cartilage or dermis). (D) Western blot performed with proteins isolated from epidermis of $Arnt^{Δ/Δ}$ pups and cultured $Arnt^{Δ/Δ}$ keratinocytes shows absence of Arnt protein, thus confirming the efficiency of gene targeting in our mouse model.

protein (Fig. 2D), thus confirming the high efficiency of gene targeting in our mouse model.

Structural and functional defects in the interfollicular epidermis of $Arnt^{Δ/Δ}$ mice

At birth, $Arnt^{Δ/Δ}$ newborns appeared normal and were indistinguishable from their littermates. Soon, however, they exhibited rapid weight loss, failed to thrive, and died within 15-30 hours after delivery. $Arnt^{Δ/Δ}$ newborns did not feed and became easily distinguishable from normal littermates, which were larger in size and were found to have milk in their stomachs (Fig. 3A-1). The inability to feed, in itself, would not explain progressive weight loss during the first hours of life in $Arnt^{Δ/Δ}$ newborns. Interestingly, rapid postnatal loss of weight is a hallmark of mice with an abnormal skin permeability barrier and extensive trans-epidermal water loss (Segre et al., 1999; Furuse et al., 2002). Using the qualitative X-gal penetration assay, we assessed skin barrier formation in $Arnt^{Δ/Δ}$ and control embryos at E18.5 when the formation of the permeability barrier should be completed (Hardman et al., 1998). Whereas control fetuses had a fully functional barrier all over the body and did not reveal X-gal penetration (Fig. 3A-2, left fetus), $Arnt^{Δ/Δ}$ fetuses (right fetus) showed profound perturbations in barrier formation. The dorsal barrier was relatively spared, whereas on the flank it was significantly reduced and absent on the ventral side of the body.

The barrier abnormalities in the epidermis of $Arnt^{Δ/Δ}$ newborns were associated with profound changes in epidermal morphology. In $Arnt^{Δ/Δ}$ skin, the epidermis was significantly thinner because of reduced overall cell number and volume. The granular layer was absent in the ventral epidermis and significantly reduced on the dorsal side of the body. Prominent parakeratosis was also seen. The cornification of keratinocytes (their transition to corny layer) was abrupt. Corneocytes were tightly attached to each other forming a solid compact mass of keratinous material (Fig. 3B-1) in contrast to the 'basket-weave' appearance of the normal corny layer (Fig. 3B-2). No morphological or functional abnormalities were detected in $Arnt^{Δ/Δ}$ HFs during the initial stages of post-natal HF morphogenesis (P1).

In order to determine potential long-term consequences of Arnt ablation to the HFs, we grafted the skin of Arnt-null newborns on immunocompromised SCID mice. Histology revealed a moderate delay in hair growth 30 days after grafting (Fig. 3C-1,2) but no structural abnormalities were seen in Arnt-deficient HFs (Fig. 3C-5,6). Immunohistochemistry with anti-Arnt antibodies in $Arnt^{Δ/Δ}$ grafts confirmed the absence of Arnt protein in the epithelial (K14-positive) cell populations (epidermis, HF matrix and epithelial sheaths, sebaceous gland), whereas as expected the mesenchymal (K14-negative) compartment including dermal fibroblasts, perifollicular dermal sheath and FP cells, expressed Arnt at the same level as in control skin (Fig. 3C-3-6). Therefore, grafting of $Arnt^{Δ/Δ}$ skin on SCID mice illustrated that application of Cre-loxP

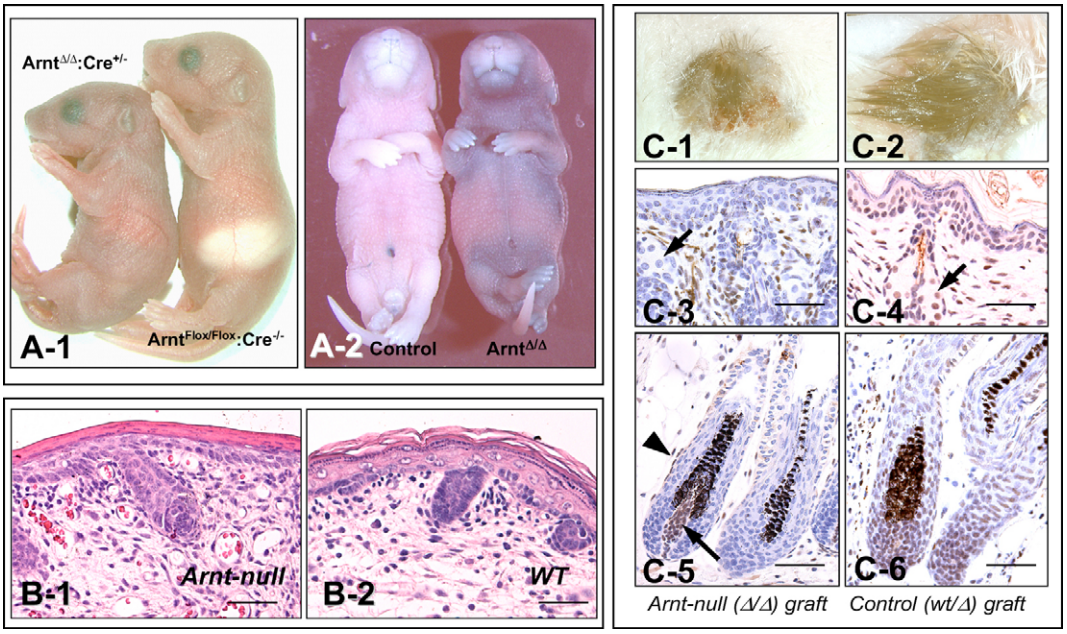

Fig. 3. Arnt-null skin phenotype in mice. (A-1) The *Arnt*$^{\Delta/\Delta}$:Cre^{+} newborn (on the left) is smaller and does not have milk in its stomach in contrast to control littermate (on the right; milk is seen through transparent skin). (A-2) Skin permeability assay (X-gal) in *Arnt*$^{flox/flox}$ (Cre^{-}) and *Arnt*$^{\Delta/\Delta}$ fetuses (E18.5). In *Arnt*$^{\Delta/\Delta}$ fetuses, the permeability barrier is impaired with most effect in the throat, chest and groin regions. Control fetus (on the left) has a fully functional barrier and does not show any X-gal penetration. (B) Skin histology (Hematoxylin and Eosin staining) in *Arnt*$^{\Delta/\Delta}$ (B-1) and control (B-2) newborn mice. Note the thinner epidermis, loss of the granular layer, compact corny layer and prominent parakeratosis in *Arnt*$^{\Delta/\Delta}$ epidermis. (C) Grafting of Arnt-null skin onto SCID mice. 30 days after grafting, *Arnt*$^{\Delta/\Delta}$ grafts (C-1) show lower rates of hair growth compared to control grafts (C-2). (C-3) Immunohistochemistry with anti-Arnt antibodies revealed the total absence of Arnt expression in epithelial (K14-positive) compartment of Arnt-null skin including sebaceous gland (arrows) and HF (C-5) whereas the mesenchymal component including dermal fibroblasts, perifollicular dermal sheath and dermal papilla cells of the HF (K14-negative structures) are positive for Arnt. Control skin had normal patterns of Arnt expression in both, epithelial and mesenchymal compartments (C-4,C-6). No difference in HF morphology between Arnt-null and wild-type grafts was observed. Bars, 40 μm.

methodology in our model provides not only an efficient (Fig. 2D), but also a long-lived deletion of Arnt in both the epidermis and in the epithelial portion of the HF.

Ultrastructural abnormalities in the interfollicular epidermis of *Arnt*$^{\Delta/\Delta}$ mice

Low magnification (×100) scanning electron microscopy (SEM) showed that the surface of ventral *Arnt*$^{\Delta/\Delta}$ epidermis was flat and taut, whereas the epidermis of control newborns was extensively folded forming prominent longitudinal ridges (Fig. 4A,B). At high magnification SEM, other striking differences were apparent. First, the surface of corneocytes in the control epidermis was perfectly smooth (not shown), whereas *Arnt*$^{\Delta/\Delta}$ epidermis had a rough, irregular and often perforated surface (Fig. 4C,D). The surface squames in *Arnt*$^{\Delta/\Delta}$ epidermis often showed the presence of retained nuclei (Fig. 4C, arrow), providing further evidence of parakeratosis revealed by light microscopy (Fig. 3B-1).

Transmission electron microscopy (TEM) identified fragments of cytoplasmic organelles in the upper corny layer of *Arnt*$^{\Delta/\Delta}$ skin (Fig. 4E,F, white arrowheads) suggesting incomplete terminal differentiation of keratinocytes. This observation is consistent with the presence of the nuclei in the surface corneocytes of *Arnt*$^{\Delta/\Delta}$ epidermis. Compared to the normal corny layer in the skin of Cre-negative control newborns (Fig. 4G), the corneocytes in *Arnt*$^{\Delta/\Delta}$ epidermis were much thicker and were tightly packed together (Fig. 4E). The cornified envelope in the control corneocytes was well-structured with internal (dark) and outer (translucent) layers (Fig. 4H, small black arrowheads) but the cornified envelope in *Arnt*$^{\Delta/\Delta}$ corneocytes was blurry and often discontinuous (Fig. 4F, small black arrowheads). Strikingly, whereas corneosomes of the normal epidermis were degraded in the lower part of corny layer (Fig. 4H, black arrows), in *Arnt*$^{\Delta/\Delta}$ skin, they were intact even in the outermost cells of the corny layer, resulting in abnormally strong cohesion between the corneocytes (Fig. 4F, black arrows) and abrogated desquamation.

Altered expression of cornified envelope proteins in *Arnt*$^{\Delta/\Delta}$ epidermis

In order to substantiate our histological and ultrastructural findings, we assessed expression of several major markers of keratinocyte differentiation in Arnt-null and control skin at the protein level using immunohistochemistry. In control epidermis, filaggrin was localized to all cells of the granular layer and loricrin was seen in the upper suprabasal, granular, and lowermost corny layer (Fig. 5A,C). In *Arnt*$^{\Delta/\Delta}$ epidermis, expression of both these proteins was observed only in occasional, flattened cells, positioned just beneath the malformed corny layer (Fig. 5B,D arrows) suggesting the abrupt cornification of *Arnt*$^{\Delta/\Delta}$ epidermis. By contrast, involucrin expression in *Arnt*$^{\Delta/\Delta}$ epidermis occupied the entire

corny layer, whereas in normal epidermis it was seen only in the thin layer of cells separating the granular and corny layers (Fig. 5E,F). The same pattern of changes, albeit less prominent, was observed in the tongue epithelium, which is K14-positive and thus also Arnt-deficient in $Arnt^{\Delta/\Delta}$ newborns. Of interest, tongue papillae in $Arnt^{\Delta/\Delta}$ pups were abnormal in shape and lacked anterior-posterior polarity (Fig. 5G,H) thus reflecting deregulation of keratinization as seen also in the corny layer of the epidermis.

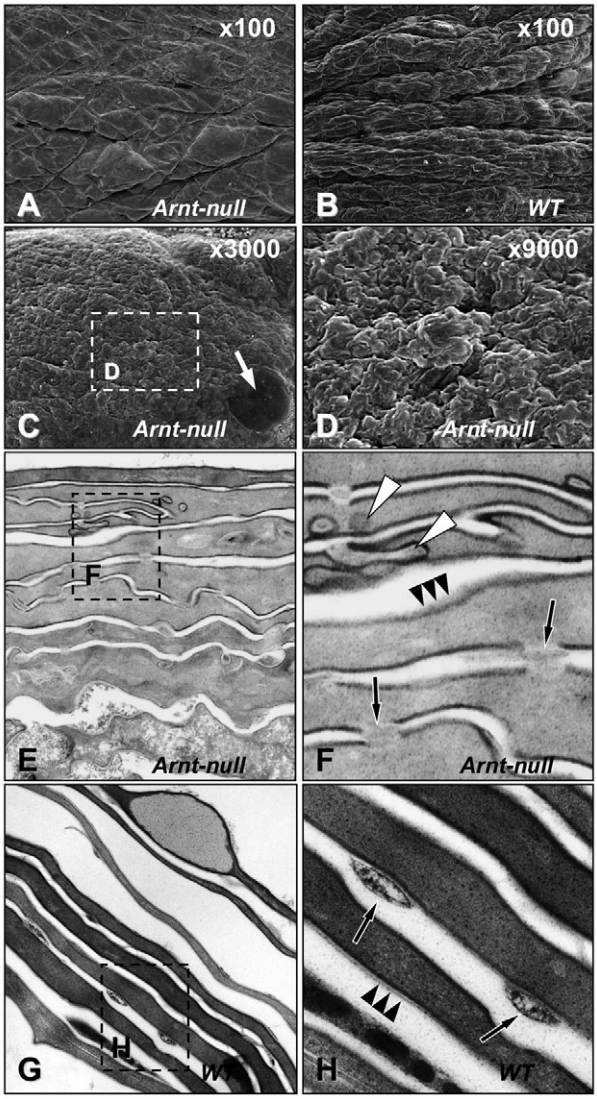

Fig. 4. (A-D) Scanning electron microscopy of the skin surface in $Arnt^{\Delta/\Delta}$ (A,C,D) and control (B) mouse newborns. The surface of $Arnt^{\Delta/\Delta}$ epidermis is flat and taut (A) whereas control epidermis is extensively folded, forming longitudinal ridges (B). At high magnification, corneocytes in the control epidermis have a perfectly smooth surface (not shown), whereas in $Arnt^{\Delta/\Delta}$ skin surface of outermost cells is rough, irregular, and often perforated (C,D). Surface cells in $Arnt^{\Delta/\Delta}$ epidermis often contain nuclei (C, arrow) suggestive of parakeratosis. (E-H) Transmission electron microscopy identified fragments of cytoplasmic organelles in the upper corny layer of $Arnt^{\Delta/\Delta}$ epidermis (F, white arrowheads). Corneocytes in $Arnt^{\Delta/\Delta}$ epidermis are much thicker and are tightly packed together (compare E with G). Whereas in normal epidermis (H) corneosomes are degraded in the lower part of corny layer (arrows), in $Arnt^{\Delta/\Delta}$ skin (F), corneosomes are intact even in the outermost portion of the corny layer (arrows) thus providing strong bonds between corneocytes. Black arrowheads in F and H indicate cornified envelope.

Real-time PCR analysis revealed slight (not significant) increase in the level of involucrin (*Ivl*) and significant decline of loricrin (*Lor*) and filaggrin (*Flg*) mRNA in $Arnt^{\Delta/\Delta}$ epidermis (Fig. 6A).

Gene expression profiling reveals deregulation of corneosome degradation machinery, lipid metabolism and cornification in $Arnt^{\Delta/\Delta}$ epidermis

To probe more deeply into the molecular basis of the epidermal phenotypes in Arnt-null mice and identify possible targets of Arnt, we compared gene expression profiles in the epidermis of $Arnt^{\Delta/\Delta}$:K14Cre^{+} (Arnt-null), $Arnt^{wt/\Delta}$:K14Cre^{+} (Arnt-heterozygote with 50% of normal Arnt activity), and littermate control ($Arnt^{flox/flox}$:K14Cre^{-}) newborn mouse females using GeneChip® Mouse Genome 430A 2.0 Arrays. The differentially expressed genes were defined as having P values below 0.00015 and the $\log_2$ expression ratios outside the –1 to 1 interval. The distribution of the expression ratios for 159 differentially expressed genes was asymmetrical and shifted towards the upregulation in the $Arnt^{\Delta/\Delta}$ epidermis with the ratio of upregulated to downregulated genes as 2.3.

Analysis of gene expression profiles showed that a substantial number of differentially expressed genes related to skin homeostasis fell into several well-defined functional groups, including cornified envelope components – ten genes; ceramide metabolism – two genes; epithelial host defense – two genes; corneosome stability – four genes. A list of genes derived from the gene expression analysis and relevant to epidermal differentiation and function is provided in Table 1. The complete list of differentially expressed genes is provided in Table S1 in supplementary material.

The most significantly upregulated genes reside within EDC on mouse chromosome 3, and are essential in formation of the cornified envelope at advanced stages of terminal differentiation. Among these genes were the members of the Sprr gene family: *Sprr1a* (+6.7), *Sprr2f* (+67.6), *Sprr2h* (+3.6), *Sprr2i* (+46.2), *Sprr2j* (+54.9), *Sprrl1* (small proline rich-like 1, +38.3) and members of the S100 gene family: *S100a8* (+46.2), *S100a9* (+41.4), and *S100a10* (+2).

Elevated levels of keratin 6 (+13.9) and keratin 16 (+3.7), which are markers of an alternative pathway of keratinocyte differentiation (Olsen et al., 1995), further confirms an abnormal terminal differentiation in the epidermis of $Arnt^{\Delta/\Delta}$ newborns.

In Arnt-null epidermis, we found significant upregulation of a number of serine protease inhibitors including *Slpi* (+13.0 fold), *Serpine1* (+22.6 fold), and *Serpinb6c* (+3.5 fold), which play a role in deactivation of stratum corneum serine proteases (Franzke et al., 1996).

Our results also showed downregulation in Arnt-null epidermis of *Asah3* (–2.03) and *Ugt8a* (–2.22) gene expression, which code for *N*-acylsphingosine amidohydrolase (alkaline ceramidase) and ceramide glucosyltransferase, respectively, both are known to play an important role in ceramide metabolism (Madison et al., 1998; Mao et al., 2003).

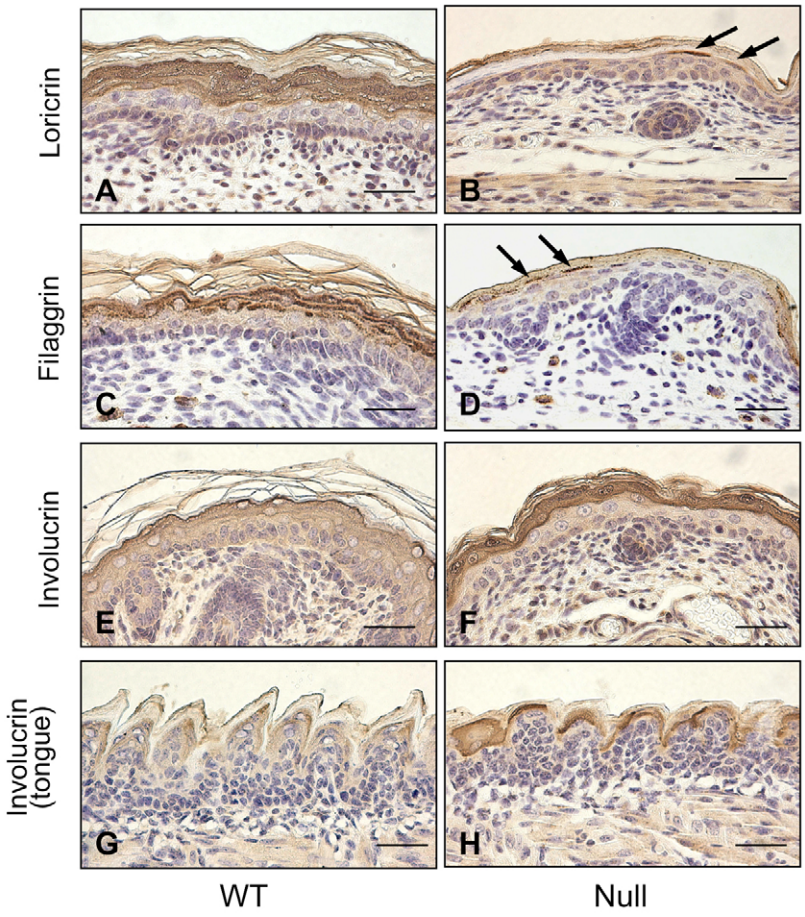

Fig. 5. Expression of cornified envelope proteins (loricrin, filaggrin and involucrin) in paraffin sections of skin and tongue in control (A,C,E,G) and Arnt-null (B,D,F,H) mouse newborns. Note the abnormal corny layer and loss of anterior-posterior polarity in the tongue papillae in the $Arnt^{\Delta/\Delta}$ newborns. Bars, 20 μm.

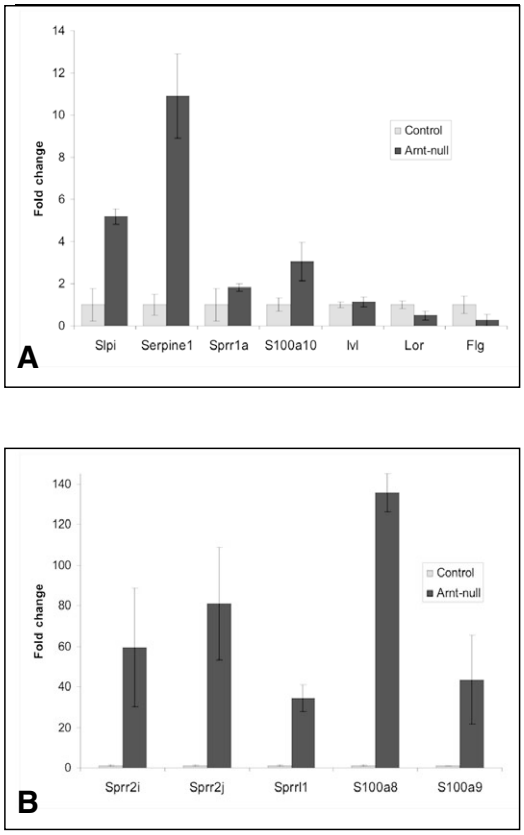

Fig. 6. Results from real-time PCR for epidermal differentiation complex genes and serine protease inhibitors performed with mRNA isolated from Arnt-null and control newborn mouse epidermis. (A) Genes with magnitude of expressional changes at or below 10. (B) Genes with magnitude of expressional changes significantly above 10.

Microarray data for certain differentially expressed epidermal genes were validated using real-time PCR assay (Fig. 6A,B).

Ceramide composition in the interfollicular epidermis of $Arnt^{\Delta/\Delta}$ mice

On the basis of previous data (Takagi et al., 2003), and the downregulation of *Asah3* and *Ugt8a* genes revealed by our microarray studies, we assumed that deregulation of lipid turnover may be one of the mechanisms causing epidermal barrier failure in our $Arnt^{\Delta/\Delta}$ mouse model. Therefore, we used high-performance thin-layer chromatography (HPTLC) to analyze the ceramide composition in the epidermis of control ($Arnt^{flox/flox}$:K14Cre^{-}) and Arnt-null ($Arnt^{\Delta/\Delta}$:K14Cre^{+}) newborn mice. In $Arnt^{\Delta/\Delta}$ epidermis, the levels of the ceramide species Cer[NS] and Cer[NH] were 3.2 and 1.9 times higher, respectively, whereas the level of Cer[AS] was 2.0 times lower (Fig. 7). Since Cer[NS] is one of the two (together with Cer[EOS]) major ceramide species in mouse epidermis, normally making up more than 30% of the total ceramide content, its 3.2-fold increase in $Arnt^{\Delta/\Delta}$ epidermis results in a pronounced alteration of the relative composition of ceramide fractions

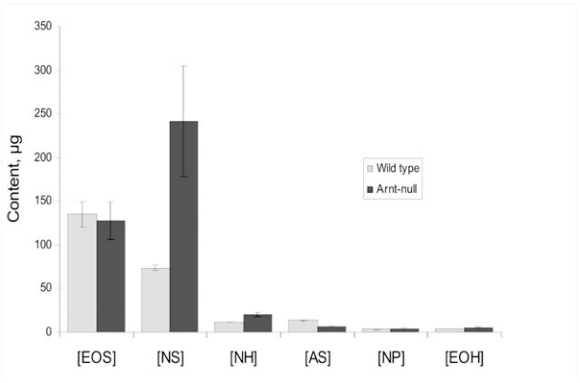

Fig. 7. The content (by weight) of the major ceramide species in the epidermis of $Arnt^{\Delta/\Delta}$ (black bars) and control (gray bars) mouse newborns (from HPTLC).

even though the differences in absolute content of such ceramide fractions as [EOS], [NP] and [EOH] between $Arnt^{\Delta/\Delta}$ and control newborn mouse epidermis were not statistically significant.

Table 1. List of genes derived from the microarray hybridization analysis with possible relevance to the barrier function ($Arnt^{\Delta/\Delta}$:Cre^{+} versus $Arnt^{flox/flox}$:Cre^{-})

UniGene	Gene name	Fold change	Affymetrix probe set
Cornified envelope components			
Sprr2a	Small proline-rich protein 2a	–3.05, –2.99	1439016_x_at, 1450618_a_at
Sprr2f	Small proline-rich protein 2f	67.65	1449833_at
Sprr2j	Small proline-rich protein 2j	54.95	1450811_at
Sprr2i	Small proline-rich protein 2i	46.21	1422963_at
Sprrl1	Small proline-rich-like 1	38.32	1456001_at
Sprr1a	Small proline-rich protein 1a	6.68	1449133_at
Sprr2h	Small proline-rich protein 2h	3.58	1422240_s_at
S100a8	S100 calcium binding protein A8 (calgranulin A)	46.21	1419394_s_at
S100a9	S100 calcium binding protein A9 (calgranulin B)	41.36	1448756_at
S100a10	S100 calcium binding protein A10 (calpactin)	2.06	1416762_at
Ceramide metabolism			
Asah3	N-acylsphingosine amidohydrolase (alkaline ceramidase) 3	–2.03	1450825_at
Ugt8	UDP-glucuronosyltransferase 8	–2.22	1419063_at
Epithelial host defense proteins			
Defb1	Defensin β1	3.78, 2.31	1419492_s_at, 1419491_at
Defb3	Defensin β3	24.93	1421806_at
Corneosome stability			
Prss35	Protease, serine 35	–4.92	1434195_at
Slpi	Secretory leukocyte protease inhibitor	13.0	1448377_at
Serpine1	Serine (cysteine) proteinase inhibitor, clade E, member 1	22.63	1419149_at
Serpinb6c	Serine (or cysteine) proteinase inhibitor, clade B, member 6c	3.48	1451594_s_at

Discussion

Taken together, the dynamic changes in Arnt expression in the skin during the early stages of normal mouse postnatal development, the striking epidermal phenotype and demise of $Arnt^{\Delta/\Delta}$ newborns, suggest that Arnt plays an essential role in control of physiological adaptation during the transition from an 'in utero' environment to a terrestrial life. The most critical elements in this process are establishing the functional epidermal barrier and acquiring the ability to feed. Both of these processes are impaired in Arnt-null mice. The inability of $Arnt^{\Delta/\Delta}$ newborns to feed could be attributed to morphological changes in the tongue and oral cavity epithelia. The impairment of the epidermal barrier in $Arnt^{\Delta/\Delta}$ newborn mice was associated with defects in critical components of epidermal homeostasis including corneosome degradation (desquamation), lipid composition and cornified envelope formation.

Corneosome retention and impeded desquamation in Arnt-null epidermis

One of the most remarkable features of Arnt-null phenotype in mice is the abnormally dense structure of the corny layer where corneocytes are tightly packed, forming a rigid keratinous structure which is strikingly different from the 'basket-weave' appearance of the corny layer in normal mouse skin (Fig. 3B1-2). The inhibition of desquamation in $Arnt^{\Delta/\Delta}$ epidermis is attributed to the abnormal retention of corneosomes (Fig. 4F). Since the microscopic structure of corneosomes was apparently normal, and we observed no changes in the expression of corneosome-specific proteins, we hypothesized that the mechanisms leading to the retention of corneosomes could be lack of an enzymatic activity.

Corneosomes are a specialized type of desmosomes consisting of macromolecular glycoprotein complexes incorporated into the cornified envelope. Their major functional components are transmembrane glycoproteins of the cadherin family, Dsg1 and Dsc1 (Serre et al., 1991; Rawlings and Matts, 2005), and a specific corneosomal protein corneodesmosin (Rawlings et al., 1994; Simon et al., 1997). In normal epidermis, corneosomes provide a connection between corneocytes in the lowermost stratum corneum, and their gradual degradation upon ascension towards the surface of the corny layer eventually leads to desquamation (Rawlings et al., 1994). The degradation of corneosomes is driven by tightly regulated action of specific hydrolytic enzymes that break down corneosomal linkages. Among these enzymes are the stratum corneum chymotryptic and tryptic enzymes (SCCE and SCTE), stratum corneum thiol protease (SCTP or cathepsin L-2), cathepsin E, and cathepsin D (reviewed by Rawlings and Matts, 2005). Endoglucosidases including heparanase 1 (Bernard et al., 2001) and other enzymes are also known to play a role in corneosome degradation. Corneodesmosin, one of the major corneosomal components secreted by lamellar bodies during desmosome-to-corneosome transformation (Rawlings et al., 1994), also undergoes desquamation-associated proteolytic degradation, which appears to be inhibited by calcium (Rawlings and Matts, 2005).

In Arnt-null epidermis, we did not observe any changes in expression of these enzymes. However, we found significant upregulation of *Slpi* (Table 1, Fig. 6A), a secretory leukocyte protease inhibitor, which is believed to be the major physiological inhibitor of SCCE (Franzke et al., 1996). In $Arnt^{\Delta/\Delta}$ epidermis we also found a prominent increase in two other serine protease inhibitors, *Serpine1* and *Serpinb6c* (22.6- and 3.5-fold, respectively). Although serpins possess high anti-serine protease activity, they were not thought to be physiologically relevant to corneosome degradation because of their low concentration in the normal corny layer (Franzke et al., 1996; Rawlings and Matts, 2005). However, the marked upregulation of these genes in $Arnt^{\Delta/\Delta}$ epidermis suggests their

potential role in inhibition of serine proteases and corneosome retention in our model.

The retention of corneosomes and subsequent abnormal desquamation is a characteristic feature of a number of skin cornification disorders (Elias et al., 2004). These diseases are also characterized by incomplete keratinocyte differentiation and impaired permeability barrier, suggesting the potential involvement of an Arnt-dependent pathway(s) in the pathogenesis of some cornification/barrier disorders in humans.

Ceramide composition in the epidermis of *Arnt*$^{\Delta/\Delta}$ newborn mice

Permeability barrier formation in mammalian epidermis requires the dimensional organization of different non-polar lipids including ceramides (Cer), free fatty acids and cholesterol into the extracellular lamellar membrane within the stratum corneum interstices (reviewed by Landmann, 1988; Elias and Menon, 1991). Although successive stages of epidermal lipid metabolism are currently well understood and their significance for corny layer mechanical integrity and barrier function is well established (Holleran et al., 1994; Mao-Qiang et al., 1996; Schmuth et al., 2000), little is known about the molecular mechanisms that govern lipid processing during formation of the epidermal barrier.

HPTLC analysis of the lipids isolated from Arnt-null newborn mouse epidermis showed a significant shift in ceramide composition. It is generally accepted that ceramides are essential for maintaining stratum corneum lamellar structures (Bouwstra et al., 1998) and barrier function (Behne et al., 2000). Thus, a marked increase in Cer[NS], one of two major ceramide species, and associated alteration of the total ceramide profile may be related to the barrier impairment in *Arnt*$^{\Delta/\Delta}$ epidermis. The downregulation of alkaline ceramidase *Asah3* (*N*-acylsphingosine amidohydrolase 3 or Cer1) and *Ugt8a* (UDP galactosyltransferase 8A or ceramide glucosyltransferase) on our microarray experiments is consistent with this proposition. Asah3 is a lysosomal enzyme that degrades ceramide into sphingosine, thus playing a role in regulating the levels of bioactive ceramides and sphingosine-1-phosphate (S1P), as well as complex sphingolipids (Mao et al., 2003) whereas Ugt8a plays a role in conversion of ceramides to glucosylceramides in the Golgi apparatus (Madison et al., 1998).

Our finding of significant upregulation of the major Cer[NS] fraction in *Arnt*$^{\Delta/\Delta}$:K14-Cre^{+} mouse epidermis is consistent with the recent work by Takagi et al. who showed that keratin 5-driven ablation of Arnt in mouse epidermis results in downregulation of dihydroceramide desaturase, Des-2 (Takagi et al., 2003), which is the key regulator of desaturation/hydroxylation of Cer[NS] but not Cer[EOS] (Ternes et al., 2002). Nevertheless, HPLC/ion-trap mass spectrometry performed by Takagi et al. showed a prominent decrease in [EOS], [NP] and [AS] ceramide fractions with no difference in Cer[NS] (Takagi et al., 2003). Whereas Takagi et al. reported decreased transcript levels of Des-2 in cultured primary Arnt-null mouse keratinocytes, expression of the Des-2 gene was not altered in our microarray analysis, which was performed with mRNA samples isolated from the epidermis of neonatal Arnt-null and control mice. Thus, our Arnt mouse model showed a somewhat different pattern of ceramide changes – upregulation of [NS] and [NH] fractions coupled with downregulation of the *Asah3* and *Ugt8a* genes, as well as a prominent shift in EDC gene expression and corneosome retention. The phenotypic differences between our and Takagi's (Takagi et al., 2003) model may be due to the use of different promoters to drive expression of Cre recombinase, i.e. K5 versus K14, which are expressed at slightly different stages of epidermal development. Alternatively, these differences may be attributable, at least in part, to the different genetic background of Cre transgenic animals utilized in both studies.

Alterations in epidermal ceramide composition are associated with several skin disorders, including atopic dermatitis and psoriasis (Hara et al., 2000; Motta et al., 1994). These observations, together with the key role of ceramides in regulation of epithelial cell growth, apoptosis, differentiation and in microvascular cell homeostasis (Geilen et al., 1997), justify the need for further studies on the role of Arnt in epidermal ceramide turnover.

Expression of cornified envelope proteins is deregulated in *Arnt*$^{\Delta/\Delta}$ skin

The presence of cytoplasmic organelles and nuclei in the upper corny layer of *Arnt*$^{\Delta/\Delta}$ epidermis (parakeratosis) is a cardinal sign of abnormal differentiation that prompted us to compare the expression of basic differentiation markers in *Arnt*$^{\Delta/\Delta}$ and control newborn mouse skin. Immunohistochemistry showed that the morphological abnormalities in *Arnt*$^{\Delta/\Delta}$ epidermis are concomitant with changes in expression of involucrin, filaggrin and loricrin. The same abnormalities were observed in the upper tongue epithelium in *Arnt*$^{\Delta/\Delta}$ newborns (Fig. 5). These changes in expression of differentiation markers in the tongue epithelium are reflected in the abnormal structure of tongue papillae which, at least in part, may explain the inability of *Arnt*$^{\Delta/\Delta}$ newborns to feed normally.

To assess changes in expression of epidermal genes resulting from Arnt ablation, we performed microarray hybridization on samples isolated from the epidermis of Arnt-null, heterozygote with 50% of normal Arnt activity, and control mouse newborns. Unexpectedly, in *Arnt*$^{\Delta/\Delta}$ epidermis we found significant upregulation of many genes associated with advanced stages of keratinocyte terminal differentiation and formation of a functional barrier (Mischke et al., 1996; Olsen et al., 1995). This finding contradicts the accepted dogma that Arnt functions exclusively as a transcriptional activator. Among genes upregulated in Arnt-null epidermis were members of Sprr gene family, including *Sprr2h*, *Sprr1a*, *Sprr2i*, *Sprr2j*, *Sprr2f* and *Sprrl1*. The deletion of Arnt in mouse newborn epidermis also results in significant induction of S100 calcium binding protein mRNAs – *S100a8*, *S100a9* and *S100a10*. These genes, together with involucrin, loricrin and filaggrin, which are deregulated in *Arnt*$^{\Delta/\Delta}$ epidermis at the protein level (Fig. 5), are clustered in the same region of mouse chromosome 3, a region syntenic with a portion of human chromosome 1q21 known as the epidermal differentiation complex (EDC) (Mischke et al., 1996). Significant upregulation of numerous genes clustered together and activated at the same stage of epidermal differentiation is particularly intriguing, since the *Arnt* gene is located just telomeric to the EDC on mouse chromosome 3, and within the EDC in the syntenic region of human chromosome 1.

The wide-ranging and extensive (up to 60-fold) upregulation of a number of EDC genes in $Arnt^{\Delta/\Delta}$ epidermis could be attributed to the following: (1) a compensatory response to the loss of Arnt; (2) transactivation by Arnt of a putative EDC master repressor; and (3) a recently proposed suppressive role of Arnt in epigenetic control of expression through recruitment of histone deacetylases (Maltepe et al., 2005). The positive (2.3) ratio of upregulated to downregulated genes in $Arnt^{\Delta/\Delta}$ epidermis suggests a substantial release of expression in the absence of Arnt and thus favors the third option, whereas two others (compensation and control of a putative EDC repressor) cannot, as yet, be ruled out.

A role of Arnt in regulation of EDC genes, protease inhibitors and lipid-related enzymes may be a key to understanding the still elusive mechanism of coordinated expression of epidermal genes during late stages of terminal differentiation (Martin et al., 2004) and to further insight into pathogenesis of certain skin disorders.

Materials and Methods

Skin sample collection and immunostaining

Samples of normal human scalp skin were obtained as discarded tissue from hair transplantation procedures, fixed in 4% paraformaldehyde and embedded in paraffin. C57BL/6J mouse pups (Jackson Laboratory, Bar Harbor, ME) were killed by CO_2 asphyxiation at defined stages of HF/skin postnatal development (day 1 postpartum (P1) – early stages of HF morphogenesis; P5 – advanced HF growth; P23 – telogen). Skin of double transgenic ($Arnt^{\Delta/\Delta}$:K14Cre^{+}) Arnt-deficient mice and appropriate control samples from Cre^{-} littermates ($Arnt^{flox/flox}$:K14Cre^{-}) were harvested immediately after birth. Skin samples were embedded in Tissue-Tek medium (Miles, Elkhart, IN) and frozen at –80°C or fixed in paraformaldehyde overnight and embedded in paraffin. Deparaffinized 5-μm-thick paraffin sections and acetone-fixed 8-μm-thick frozen sections were processed for immunohistochemistry using the standard ABC (Avidin-Biotin Complex) procedure. Sections of human and mouse skin were treated with mehtanol/H_2O_2 in order to block endogenous peroxidase. For antigen retrieval, paraffin sections were boiled in a microwave for 10 minutes in antigen unmasking solution (Vector Laboratories, Burlingame, CA). Incubation with primary antibodies (Table S2 in supplementary material) was performed overnight after blocking with appropriate serum. After incubation with secondary antibodies (1:200), the signal was detected using the ABC kit (Vector Laboratories) along with Hematoxylin counterstaining. Processing of corresponding mouse skin sections with no primary or secondary antibodies was used as negative control. Photo-documentation was performed using Zeiss Axioscope microscope equipped with an appropriate set of filters and an Axiovision image analysis system (Zeiss, Thornwood, NJ). All animal experiments were approved by the Institutional Animal Care and Use Committee Review Board at the Columbia University Presbyterian Medical Center.

Generation of skin-targeted Arnt knockout mouse model using Cre-loxP methodology

Arnt-floxed mice were obtained from F. J. Gonzalez, NCI, Bethesda, DC. In these mice, two loxP sites were introduced into introns 5 and 6, thus flanking exon 6 (Fig. 2B) that encodes the bHLH region (Fig. 2A) of the *Arnt* gene (accession no. NM_009709). Transmission of the *Arnt*-floxed allele was monitored with a set of three specific primers (Fig. 2C) designed from the intron sequences flanking loxP sites (Tomita et al., 2000). The Cre recombinase-expressing construct was introduced into the *Arnt*-floxed mice by crossbreeding with K14Cre animals obtained from Elaine Fuchs, Rockefeller University, New York, NY (Vasioukhin et al., 1999). Double heterozygous ($Arnt^{wt/\Delta}$:K14Cre^{+}) females were selected and upon reaching maturity backcrossed to homozygous *Arnt*-floxed ($Arnt^{flox/flox}$:K14Cre^{-}) males.

Epidermal permeability assay

Qualitative patterns of the permeability barrier formation at the late stages of embryogenesis were assessed based on the barrier-dependent penetration of X-gal into embryonic mouse skin (Hardman et al., 1998). Freshly isolated embryos (E18.5) were immersed in X-gal reaction mix and incubated at room temperature overnight. After the staining, embryos were washed and photographed using a stereomicroscope with a Nikon digital camera.

Grafting of Arnt-deficient neonatal mouse skin on SCID mice

The dorsal skin harvested from newborn $Arnt^{\Delta/\Delta}$ and Cre-negative control pups was grafted on the back (interscapular region) of 7- to 8-week old C.B.-17/LCR Crl-SCID mice (Charles River, Cambridge, MA). Briefly, back skin of anesthetized SCID animals was shaved, repeatedly washed with 70% ethanol and sterile PBS and a 10×10 mm full-thickness skin incision was made. The freshly collected newborn skin specimens were trimmed to the size and placed on the wound. The border between the graft and the host skin was fixed with Nexaband fluid (Veterinary Product Laboratories, Phoenix, AZ) and four surgical sutures were placed at the corners of the graft. Sterile Vaseline gauze was applied on the graft surface in order to prevent drying. For the first 3 days after the surgery, animals received intramuscular injection of analgesic buprenorphin (1-2 mg/kg of body weight, twice a day), and doxycycline was added into the drinking water. Three weeks after grafting the recipient animals were killed. Skin samples from the graft areas were processed for histology and immunohistochemistry as described above. The fraction of rejected grafts was below 10%.

Cell culture

Primary mouse keratinocytes were isolated from mouse skin and cultured as described earlier (Hennings, 1994; Wu and Morris, 2005). Briefly, the epidermis of previously genotyped newborn mice was split from the dermis by overnight incubation in 0.25% trypsin-EDTA at 4°C. The epidermis was minced and incubated for 1 hour at room temperature in SMEM containing 100 μg/ml gentamicin (Invitrogen, Carlsbad, CA) with moderate stirring. After filtration, the cells were spun down at 200 ***g*** for 5 minutes and re-suspended in low Ca^{2+} (0.05 mM) keratinocyte SFM (Invitrogen) supplemented with 10% Chelex-treated FBS, EGF, BPE and 100 μg/ml gentamicin. Cell were seeded on 60-mm collagen-coated dishes (5×10^5 cells/cm^2) and cultured in a humidified incubator at 32°C and 5.0% CO_2 until they covered about 80% of the growth surface.

Western blotting

For western blotting we used protein samples isolated from cultured $Arnt^{\Delta/\Delta}$ keratinocytes and from mouse epidermis and dermis isolated from the whole skin as described above. Skin was harvested from Arnt-null pups immediately after birth and from normal C57Bl/6 mice (Jackson Laboratory, Bar Harbor, ME) at days 1, 3, 5 and 23 postpartum. Proteins were isolated by the treatment of samples with lysis buffer containing 1% NP-40, 50 mM Tris-HCl pH 7.5, 150 mM NaCl, 0.1% SDS, 0.5% sodium deoxycholate, 100 μg/ml PMSF, 25 μ g/ml aprotinin, and 62.5 μg/ml leupeptin. Lysates were incubated for 1 hour on ice with shaking, spun down at 10,000 ***g*** for 20 minutes at 4°C, and boiled with sample buffer (Bio-Rad) for 3 minutes. Proteins were resolved by denaturing electrophoresis on discontinuous polyacrylamide slab gels (SDS-PAGE) and transferred to PVDF membrane (Amersham, Piscataway, NJ) according to the manufacturer's protocol. Membranes were blocked with 5% non-fat milk in TBS-T for 1 hour at room temperature followed by overnight incubation with primary anti-Arnt antibodies (Santa Cruz Biotechnologies, CA) at 4°C, with shaking. After washing in TBS-T, membranes were incubated with the corresponding horseradish-peroxidase (HRP)-conjugated secondary antibodies for 1 hour at room temperature. The signal was visualized with an enhanced chemiluminescence (ECL) system (Amersham). Then, membranes were washed and re-probed with antibodies specific to β-actin. The western blot data were quantified by using a FluorChem 8800 digital image system (Alpha Innotech, San Leandro, CA) and normalized to the β-actin signals.

Real-time PCR

Real-time PCR analysis was performed using primary mouse keratinocytes and epidermis freshly harvested from newborn female mice. After harvesting, the epidermis was washed with cold PBS, minced and homogenized in TRIzol (Invitrogen, Carlsbad, CA). Total RNA was isolated from cells and epidermal tissue according to the manufacturer's protocol and reverse transcribed for 50 minutes at 50°C using SuperScript™ III First-Strand Synthesis System for RT-PCR (Invitrogen) and oligo(dT) primer. RT-PCR was performed using Applied Biosystems 7300 Fast real-time PCR System with SYBR GREEN PCR Master Mix (Applied Biosystems) and the primers listed in Table S3 in supplementary material. Taking into account high similarity of Sprr genes, the specificity of designed primers was ensured using Beacon Designer Software (Premier Biosoft International, Palo Alto, CA). The ABI sequence detection software (version 1.6.3) and Microsoft™ Excel were used to quantify cDNA content in the samples. The data were normalized to β-actin, chosen as an internal control.

Transmission and scanning electron microscopy

Skin samples were harvested from the ventral side of $Arnt^{\Delta/\Delta}$ and control (Cre^{-}) pups immediately after birth, fixed overnight by immersion in 2.5% glutaraldehyde in 0.1 M cacodylate buffer (pH 7.2) containing 7% sucrose at 4°C. For scanning electron microscopy (SEM), fixed samples were processed through a critical point dryer, mounted on aluminum stubs, and sputter-coated with gold-palladium alloy. Samples were analyzed using a JEOL 6400 Scanning Electron Microscope. For transmission electron microscopy (TEM), samples were postfixed in 1.3% osmium tetroxide and embedded in Epon 812 (Polysciences, Warington, PA). Ultrathin sections were stained with uranyl acetate and lead citrate and analyzed in a JEOL 100CX transmission electron microscope at an accelerating voltage of 60 kV.

Analysis of ceramide composition of newborn mouse epidermis

Total lipids were extracted from the epidermis of newborn $Arnt^{\Delta/\Delta}$ (four samples) and control (six samples) pups by the method of Bligh and Dyer, as previously described (Farwanah et al., 2002). Briefly, the epidermis from each newborn pup was lyophilized and weighed. The extraction was performed successively in chloroform:methanol, 2:1, 1:1 and 1:2 with shaking at room temperature for 3 hours. After extraction, samples were centrifuged and lipid-containing eluates were evaporated. Dried samples were stored at –20°C.

For high performance thin-layer chromatography (HPTLC), 20 μl of each sample, re-dissolved in 1 ml chloroform/methanol (1:1, v/v), were applied to silica gel 60 HPTLC plates (Merck Darmstadt, Germany), which were pre-run with a solvent system composed of chloroform:methanol (65:35, v/v). Sample were applied using an Automatic TLC Sampler 4 (Camag, Muttenz, Switzerland) at a dosage speed of 100 μl/second. Development of the plates, visualization of the bands, and the densitometry were carried out as previously reported (Farwanah et al., 2002). Identification of ceramides was performed taking into account the basic differences between mouse and human ceramides (Doering et al., 2002). Based on the previously established criteria (Wertz and Downing, 1986; Motta et al., 1993; Robson et al., 1994) the following ceramide classes have been assigned: Cer[EOS], Cer[NS], Cer[NP], Cer[EOH], Cer[NH] and Cer[AS].

Microarray analysis

To expose downstream targets of Arnt-dependent regulatory pathways in the skin, we compared gene expression profiles in the epidermis of $Arnt^{\Delta/\Delta}$ and control newborn female mice using six replicates for each of three different conditions: $Arnt^{\Delta/\Delta}$:K14Cre^{+} (Arnt-null); $Arnt^{\Delta/wt}$:K14Cre^{+} (Arnt-flox heterozygote with 50% of normal Arnt activity) and $Arnt^{flox/flox}$:K14Cre^{-} (control). Arnt-heterozygous Cre-positive samples were used as an additional control for Cre recombinase activity. Each sample was obtained from the epidermis of one female newborn and stored in RNAlater®-ICE frozen tissue transition solution (Ambion, Austin, TX) at –80°C until further use. For hybridization we used the GeneChip® Mouse Genome 430A 2.0 Array (Affymetrix, CA) containing approximately 14,000 well-characterized mouse genes. Isolation of total RNA, probe preparation, labeling and characterization were performed according to Affymetrix protocols.

The signal intensities were extracted from the CEL files, adjusted for the background and normalized by quantile normalization using probe level data analysis (RMA) algorithms implemented in R package *affy* (Gautier et al., 2004).

The genes differentially expressed between all three groups of newborns were detected using t-statistics followed by F-test implemented in Bioconductor R package *multtest* (Gentleman et al., 2004). For visualization, clustering and principal component analysis (PCA) the data were imported into Spotfire decision site for functional genomics (Spotfire, MA).

We acknowledge Elaine Fuchs, Rockefeller University, New York, NY, and Frank Gonzalez, NCI, Bethesda, DC, for kind donation of the K14:Cre and $Arnt^{flox}$ mice. We are also grateful to Vladimir Botchkarev and Andrey Sharov, Boston University, Boston, MA, for sharing the mouse skin grafting technique with us This work was supported by NIH grant (AR Y7898) to D.R.R. and by Dermatology Foundation and American Skin Association Research Grants to A.A.P.

References

Adelman, D. M., Maltepe, E. and Simon, M. C. (1999). Multilineage embryonic hematopoiesis requires hypoxic ARNT activity. *Genes Dev.* **13**, 2478-2483.

Aitola, M. H. and Pelto-Huikko, M. T. (2003). Expression of Arnt and Arnt2 mRNA in developing murine tissues. *J. Histochem. Cytochem.* **51**, 41-54.

Behne, M., Uchida, Y., Seki, T., de Montellano, P. O., Elias, P. M. and Holleran, W. M. (2000). Omega-hydroxyceramides are required for corneocyte lipid envelope (CLE) formation and normal epidermal permeability barrier function. *J. Invest. Dermatol.* **114**, 185-192.

Bernard, D., Mehul, B., Delattre, C., Simonetti, L., Thomas-Collignon, A. and Schmidt, R. (2001). Purification and characterization of the endoglycosidase heparanase 1 from human plantar stratum corneum: a key enzyme in epidermal physiology? *J. Invest. Dermatol.* **117**, 1266-1273.

Bouwstra, J. A., Gooris, G. S., Dubbelaar, F. E., Weerheim, A. M., Ijzerman, A. P. and Ponec, M. (1998). Role of ceramide 1 in the molecular organization of the stratum corneum lipids. *J. Lipid Res.* **39**, 186-196.

Crow, K. D. (1983). Significanse of cutaneous lesions in the symptomatology of exposure to dioxins and other chloracnegenes. In *Human and Environmental Risks of Chlorinated Dioxins and Related Compounds* (ed. R. E. Tucker), pp. 605-612. New York: Plenum Press.

Doering, T., Brade, H. and Sandhoff, K. (2002). Sphingolipid metabolism during epidermal barrier development in mice. *J. Lipid Res.* **43**, 1727-1733.

Elias, P. M. and Menon, G. K. (1991). Structural and lipid biochemical correlates of the epidermal permeability barrier. *Adv. Lipid Res.* **24**, 1-26.

Elias, P. M., Crumrine, D., Rassner, U., Hachem, J. P., Menon, G. K., Man, W., Choy, M. H., Leypoldt, L., Feingold, K. R. and Williams, M. L. (2004). Basis for abnormal desquamation and permeability barrier dysfunction in RXLI. *J. Invest. Dermatol.* **122**, 314-319.

Farwanah, H., Neubert, R., Zellmer, S. and Raith, K. (2002). Improved procedure for the separation of major stratum corneum lipids by means of automated multiple development thin-layer chromatography. *J. Chromatogr. B Analyt. Technol. Biomed. Life Sci.* **780**, 443-450.

Franzke, C. W., Baici, A., Bartels, J., Christophers, E. and Wiedow, O. (1996). Antileukoprotease inhibits stratum corneum chymotryptic enzyme. Evidence for a regulative function in desquamation. *J. Biol. Chem.* **271**, 21886-21890.

Furuse, M., Hata, M., Furuse, K., Yoshida, Y., Haratake, A., Sugitani, Y., Noda, T., Kubo, A. and Tsukita, S. (2002). Claudin-based tight junctions are crucial for the mammalian epidermal barrier: a lesson from claudin-1-deficient mice. *J. Cell Biol.* **156**, 1099-1111.

Gassmann, M., Kvietikova, I., Rolfs, A. and Wenger, R. H. (1997). Oxygen- and dioxin-regulated gene expression in mouse hepatoma cells. *Kidney Int.* **51**, 567-574.

Gautier, L., Cope, L., Bolstad, B. M. and Irizarry, R. A. (2004). affy–analysis of Affymetrix GeneChip data at the probe level. *Bioinformatics* **20**, 307-315.

Geilen, C. C., Wieder, T. and Orfanos, C. E. (1997). Ceramide signalling: regulatory role in cell proliferation, differentiation and apoptosis in human epidermis. *Arch. Dermatol. Res.* **289**, 559-566.

Gentleman, R. C., Carey, V. J., Bates, D. M., Bolstad, B., Dettling, M., Dudoit, S., Ellis, B., Gautier, L., Ge, Y., Gentry, J. et al. (2004). Bioconductor: open software development for computational biology and bioinformatics. *Genome Biol.* **5**, R80.

Geusau, A., Jurecka, W., Nahavandi, H., Schmidt, J. B., Stingl, G. and Tschachler, E. (2000). Punctate keratoderma-like lesions on the palms and soles in a patient with chloracne: a new clinical manifestation of dioxin intoxication? *Br. J. Dermatol.* **143**, 1067-1071.

Goda, N., Dozier, S. J. and Johnson, R. S. (2003). HIF-1 in cell cycle regulation, apoptosis, and tumor progression. *Antioxid. Redox Signal.* **5**, 467-473.

Gu, Y. Z., Hogenesch, J. B. and Bradfield, C. A. (2000). The PAS superfamily: sensors of environmental and developmental signals. *Annu. Rev. Pharmacol. Toxicol.* **40**, 519-561.

Guillemin, K. and Krasnow, M. A. (1997). The hypoxic response: huffing and HIFing. *Cell* **89**, 9-12.

Hara, J., Higuchi, K., Okamoto, R., Kawashima, M. and Imokawa, G. (2000). High-expression of sphingomyelin deacylase is an important determinant of ceramide deficiency leading to barrier disruption in atopic dermatitis. *J. Invest. Dermatol.* **115**, 406-413.

Hardman, M. J., Sisi, P., Banbury, D. N. and Byrne, C. (1998). Patterned acquisition of skin barrier function during development. *Development* **125**, 1541-1552.

Hasan, A. and Fischer, B. (2003). Epithelial cells in the oviduct and vagina and steroid-synthesizing cells in the rabbit ovary express AhR and ARNT. *Anat. Embryol.* **207**, 9-18.

Hennings, H. (1994). Primary culture of keratinocytes from newborn mouse epidermis in medium with lowered levels of Ca2+. In *Keratinocyte Methods* (ed. I. M. Leigh and F. M. Watt), pp. 21-23. Cambridge: Cambridge University Press.

Hoffman, E. C., Reyes, H., Chu, F. F., Sander, F., Conley, L. H., Brooks, B. A. and Hankinson, O. (1991). Cloning of a factor required for activity of the Ah (dioxin) receptor. *Science* **252**, 954-958.

Holleran, W. M., Takagi, Y., Menon, G. K., Jackson, S. M., Lee, J. M., Feingold, K. R. and Elias, P. M. (1994). Permeability barrier requirements regulate epidermal beta-glucocerebrosidase. *J. Lipid Res.* **35**, 905-912.

Hombach-Klonisch, S., Pocar, P., Kietz, S. and Klonisch, T. (2005). Molecular actions of polyhalogenated arylhydrocarbons (PAHs) in female reproduction. *Curr. Med. Chem.* **12**, 599-616.

Huang, P., Rannug, A., Ahlbom, E., Hakansson, H. and Ceccatelli, S. (2000). Effect of 2,3,7,8-tetrachlorodibenzo-p-dioxin on the expression of cytochrome P450 1A1, the aryl hydrocarbon receptor, and the aryl hydrocarbon receptor nuclear translocator in rat brain and pituitary. *Toxicol. Appl. Pharmacol.* **169**, 159-167.

Irizarry, R. A., Bolstad, B. M., Collin, F., Cope, L. M., Hobbs, B. and Speed, T. P. (2003). Summaries of Affymetrix GeneChip probe level data. *Nucleic Acids Res.* **31**, e15.

Jain, S., Maltepe, E., Lu, M. M., Simon, C. and Bradfield, C. A. (1998). Expression of ARNT, ARNT2, HIF1 alpha, HIF2 alpha and Ah receptor mRNAs in the developing mouse. *Mech. Dev.* **73**, 117-123.

Jones, C. L. and Reiners, J. J., Jr (1997). Differentiation status of cultured murine keratinocytes modulates induction of genes responsive to 2,3,7,8-tetrachlorodibenzo-p-dioxin. *Arch. Biochem. Biophys.* **347**, 163-173.

Kozak, K. R., Abbott, B. and Hankinson, O. (1997). ARNT-deficient mice and placental differentiation. *Dev. Biol.* **191**, 297-305.

Kuratsune, M. (1980). Yusho. In *Halogenated Biphenyls, Terphenyls, Naphthalenes, Dibenzo Dioxins, and Related Products* (ed. R. D. Kimbrough), pp. 287-302. Amsterdam: Elsevier/North Holland.

Landmann, L. (1988). The epidermal permeability barrier. *Anat. Embryol.* **178**, 1-13.

Lee, J. W., Bae, S. H., Jeong, J. W., Kim, S. H. and Kim, K. W. (2004). Hypoxia-inducible factor (HIF-1)alpha: its protein stability and biological functions. *Exp. Mol. Med.* **36**, 1-12.

Madison, K. C., Sando, G. N., Howard, E. J., True, C. A., Gilbert, D., Swartzendruber, D. C. and Wertz, P. W. (1998). Lamellar granule biogenesis: a role

for ceramide glucosyltransferase, lysosomal enzyme transport, and the Golgi. *J. Invest. Dermatol. Symp. Proc.* **3**, 80-86.

Maltepe, E., Schmidt, J. V., Baunoch, D., Bradfield, C. A. and Simon, M. C. (1997). Abnormal angiogenesis and responses to glucose and oxygen deprivation in mice lacking the protein ARNT. *Nature* **386**, 403-407.

Maltepe, E., Krampitz, G. W., Okazaki, K. M., Red-Horse, K., Mak, W., Simon, M. C. and Fisher, S. J. (2005). Hypoxia-inducible factor-dependent histone deacetylase activity determines stem cell fate in the placenta. *Development* **132**, 3393-3403.

Mao, C., Xu, R., Szulc, Z. M., Bielawski, J., Becker, K. P., Bielawska, A., Galadari, S. H., Hu, W. and Obeid, L. M. (2003). Cloning and characterization of a mouse endoplasmic reticulum alkaline ceramidase: an enzyme that preferentially regulates metabolism of very long chain ceramides. *J. Biol. Chem.* **278**, 31184-31191.

Mao-Qiang, M., Jain, M., Feingold, K. R. and Elias, P. M. (1996). Secretory phospholipase A2 activity is required for permeability barrier homeostasis. *J. Invest. Dermatol.* **106**, 57-63.

Martin, N., Patel, S. and Segre, J. A. (2004). Long-range comparison of human and mouse Sprr loci to identify conserved noncoding sequences involved in coordinate regulation. *Genome Res.* **14**, 2430-2438.

Mimura, J. and Fujii-Kuriyama, Y. (2003). Functional role of AhR in the expression of toxic effects by TCDD. *Biochim. Biophys. Acta* **1619**, 263-268.

Mischke, D., Korge, B. P., Marenholz, I., Volz, A. and Ziegler, A. (1996). Genes encoding structural proteins of epidermal cornification and S100 calcium-binding proteins form a gene complex ("epidermal differentiation complex") on human chromosome 1q21. *J. Invest. Dermatol.* **106**, 989-992.

Motta, S., Monti, M., Sesana, S., Caputo, R., Carelli, S. and Ghidoni, R. (1993). Ceramide composition of the psoriatic scale. *Biochim. Biophys. Acta* **1182**, 147-151.

Motta, S., Sesana, S., Monti, M., Giuliani, A. and Caputo, R. (1994). Interlamellar lipid differences between normal and psoriatic stratum corneum. *Acta Derm. Venereol. Suppl. Stockh.* **186**, 131-132.

Olsen, E., Rasmussen, H. H. and Celis, J. E. (1995). Identification of proteins that are abnormally regulated in differentiated cultured human keratinocytes. *Electrophoresis* **16**, 2241-2248.

Poland, A. and Knutson, J. C. (1982). 2,3,7,8-tetrachlorodibenzo-p-dioxin and related halogenated aromatic hydrocarbons: examination of the mechanism of toxicity. *Annu. Rev. Pharmacol. Toxicol.* **22**, 517-554.

Poskitt, L. B., Duffill, M. B. and Rademaker, M. (1994). Chloracne, palmoplantar keratoderma and localized scleroderma in a weed sprayer. *Clin. Exp. Dermatol.* **19**, 264-267.

Rawlings, A. V. and Matts, P. J. (2005). Stratum corneum moisturization at the molecular level: an update in relation to the dry skin cycle. *J. Invest. Dermatol.* **124**, 1099-1110.

Rawlings, A. V., Scott, I. R., Harding, C. R. and Bowser, P. A. (1994). Stratum corneum moisturization at the molecular level. *J. Invest. Dermatol.* **103**, 731-741.

Reyes, H., Reisz-Porszasz, S. and Hankinson, O. (1992). Identification of the Ah receptor nuclear translocator protein (Arnt) as a component of the DNA binding form of the Ah receptor. *Science* **256**, 1193-1195.

Robson, K. J., Stewart, M. E., Michelsen, S., Lazo, N. D. and Downing, D. T. (1994). 6-Hydroxy-4-sphingenine in human epidermal ceramides. *J. Lipid Res.* **35**, 2060-2068.

Schmidt, J. V. and Bradfield, C. A. (1996). Ah receptor signaling pathways. *Annu. Rev. Cell Dev. Biol.* **12**, 55-89.

Schmuth, M., Man, M. Q., Weber, F., Gao, W., Feingold, K. R., Fritsch, P., Elias, P. M. and Holleran, W. M. (2000). Permeability barrier disorder in Niemann-Pick disease: sphingomyelin-ceramide processing required for normal barrier homeostasis. *J. Invest. Dermatol.* **115**, 459-466.

Segre, J. A., Bauer, C. and Fuchs, E. (1999). Klf4 is a transcription factor required for establishing the barrier function of the skin. *Nat. Genet.* **22**, 356-360.

Serre, G., Mils, V., Haftek, M., Vincent, C., Croute, F., Reano, A., Ouhayoun, J. P., Bettinger, S. and Soleilhavoup, J. P. (1991). Identification of late differentiation antigens of human cornified epithelia, expressed in re-organized desmosomes and bound to cross-linked envelope. *J. Invest. Dermatol.* **97**, 1061-1072.

Simon, M., Montezin, M., Guerrin, M., Durieux, J. J. and Serre, G. (1997). Characterization and purification of human corneodesmosin, an epidermal basic glycoprotein associated with corneocyte-specific modified desmosomes. *J. Biol. Chem.* **272**, 31770-31776.

Takagi, S., Tojo, H., Tomita, S., Sano, S., Itami, S., Hara, M., Inoue, S., Horie, K., Kondoh, G., Hosokawa, K. et al. (2003). Alteration of the 4-sphingenine scaffolds of ceramides in keratinocyte-specific Arnt-deficient mice affects skin barrier function. *J. Clin. Invest.* **112**, 1372-1382.

Taylor, B. L. and Zhulin, I. B. (1999). PAS domains: internal sensors of oxygen, redox potential, and light. *Microbiol. Mol. Biol. Rev.* **63**, 479-506.

Ternes, P., Franke, S., Zahringer, U., Sperling, P. and Heinz, E. (2002). Identification and characterization of a sphingolipid delta 4-desaturase family. *J. Biol. Chem.* **277**, 25512-25518.

Tomita, S., Sinal, C. J., Yim, S. H. and Gonzalez, F. J. (2000). Conditional disruption of the aryl hydrocarbon receptor nuclear translocator (Arnt) gene leads to loss of target gene induction by the aryl hydrocarbon receptor and hypoxia-inducible factor 1alpha. *Mol. Endocrinol.* **14**, 1674-1681.

Vasioukhin, V., Degenstein, L., Wise, B. and Fuchs, E. (1999). The magical touch: genome targeting in epidermal stem cells induced by tamoxifen application to mouse skin. *Proc. Natl. Acad. Sci. USA* **96**, 8551-8556.

Wanner, R., Panteleyev, A., Henz, B. M. and Rosenbach, T. (1996). Retinoic acid affects the expression rate of the differentiation- related genes aryl hydrocarbon receptor, ARNT and keratin 4 in proliferative keratinocytes only. *Biochim. Biophys. Acta* **1317**, 105-111.

Wertz, P. W. and Downing, D. T. (1986). Linoleate content of epidermal acylglucosylceramide in newborn, growing and mature mice. *Biochim. Biophys. Acta* **876**, 469-473.

Wu, W. Y. and Morris, R. J. (2005). Method for the harvest and assay of in vitro clonogenic keratinocytes stem cells from mice. *Methods Mol. Biol.* **289**, 79-86.

Xu, C., Li, C. Y. and Kong, A. N. (2005). Induction of phase I, II and III drug metabolism/transport by xenobiotics. *Arch. Pharm. Res.* **28**, 249-268.

Supplementary Table S1. Differentially expressed genes

Probe Set ID	Gene Symbol	t-test/Anova	AvgR	Gene Title
1419230_at	Krt1-12	2.36E-07	-3.712063	keratin complex 1, acidic, gene 12
1419231_s_at	Krt1-12	3.66E-07	-3.677800433	keratin complex 1, acidic, gene 12
1418649_at	Egln3	1.21E-08	-3.2664529	EGL nine homolog 3 (C. elegans)
1434195_at	Prss35	0.00063239	-2.3044876	protease, serine, 35
1418648_at	Egln3	1.23E-05	-2.278906233	EGL nine homolog 3 (C. elegans)
1422257_s_at	Cyp2b10	0.000188646	-2.278152933	cytochrome P450, family 2, subfamily b, polypeptide 10
1449365_at	Edg8	0.000113168	-2.020486833	endothelial differentiation, sphingolipid G-protein-coupled receptor, 8
1425645_s_at	Cyp2b10	4.80E-05	-2.0114634	cytochrome P450, family 2, subfamily b, polypeptide 10
1450645_at	Mt4	0.000101685	-1.9760637	metallothionein 4
1422188_s_at	Tcrg	0.00011625	-1.954218867	T-cell receptor gamma chain /// T cell receptor gamma chain
1438244_at	Nfib	0.000297612	-1.888168733	nuclear factor I/B
1455961_at	Mme	9.19E-05	-1.818924367	Membrane metallo endopeptidase
1416390_at	Rcbtb2	0.001067669	-1.7334055	regulator of chromosome condensation and BTB domain containing protein 2
1417266_at	Ccl6	9.15E-07	-1.725338533	chemokine (C-C motif) ligand 6
1416481_s_at	Higd1a	0.000135494	-1.724358633	HIG1 domain family, member 1A
1453360_a_at	Tex9	0.000636579	-1.703543333	testis expressed gene 9
1436566_at	Rab40b	4.86E-05	-1.6680399	Rab40b, member RAS oncogene family
1418219_at	Il15	0.000124253	-1.641713967	interleukin 15
1426340_at	Slc1a3	8.94E-05	-1.636747167	solute carrier family 1 (glial high affinity glutamate transporter), member 3
1418826_at	Ms4a6b	0.000106146	-1.6175151	membrane-spanning 4-domains, subfamily A, member 6B
1439016_x_at	Sprr2a	3.89E-05	-1.6052376	small proline-rich protein 2A
1450618_a_at	Sprr2a	2.35E-04	-1.5836734	small proline-rich protein 2A
1422542_at	Gpr34	0.000361524	-1.561782767	G protein-coupled receptor 34
1448502_at	Slc16a7	3.36E-05	-1.500206033	solute carrier family 16 (monocarboxylic acid transporters), member 7
1448359_a_at	Higd1a	2.48E-05	-1.465078967	HIG1 domain family, member 1A
1420249_s_at	Ccl6	4.59E-07	-1.448485733	chemokine (C-C motif) ligand 6
1451454_at	Pcdh20	0.00203199	-1.443424633	protocadherin 20
1450430_at	Mrc1	0.001047084	-1.439210633	mannose receptor, C type 1
1423433_at	Trove2	0.001065967	-1.4106575	TROVE domain family, member 2
1448551_a_at	Trim2	1.71E-06	-1.395877967	tripartite motif protein 2
1424410_at	Ttc8	0.00011408	-1.3700274	tetratricopeptide repeat domain 8
1427168_a_at	Col14a1	1.82E-05	-1.352811867	procollagen, type XIV, alpha 1
1460197_a_at	Steap4	0.000228778	-1.325791	STEAP family member 4
1426787_at	Sfi1	0.000896628	-1.321994433	Sfi1 homolog, spindle assembly associated (yeast)
1427655_a_at	A630038E17Rik	0.000895618	-1.2983144	RIKEN cDNA A630038E17 gene
1450616_at	Ear5	2.55E-05	-1.2816092	eosinophil-associated, ribonuclease A family, member 5
1417028_a_at	Trim2	0.000126701	-1.271967167	tripartite motif protein 2
1455700_at	Mterfd3	0.000248432	-1.2592221	MTERF domain containing 3
1415756_a_at	Snapap	9.70E-05	-1.241414967	SNAP-associated protein
1416053_at	Lrrn1	0.001307997	-1.239794667	leucine rich repeat protein 1, neuronal
1426622_a_at	Qpct	0.000122179	-1.2310838	glutaminyl-peptide cyclotransferase (glutaminyl cyclase)
1421937_at	Dapp1	0.000455443	-1.2160661	dual adaptor for phosphotyrosine and 3-phosphoinositides 1
1450770_at	3632451O06Rik	0.000538847	-1.2115839	RIKEN cDNA 3632451O06 gene
1438887_a_at	Gcl	0.000364422	-1.192778133	germ cell-less homolog (Drosophila)
1422954_at	Zfp60	0.000359924	-1.184648267	zinc finger protein 60
1416151_at	Sfrs3	0.00222128	-1.180315933	splicing factor, arginine/serine-rich 3 (SRp20)
1420409_at	Krt1-24	0.001202231	-1.1634596	keratin complex 1, acidic, gene 24
1419063_at	Ugt8a	0.002162591	-1.152453967	UDP galactosyltransferase 8A
1418915_at	1810037K07Rik	0.000930549	-1.150172667	RIKEN cDNA 1810037K07 gene
1451050_at	Nt5c3	4.55E-05	-1.144837433	5'-nucleotidase, cytosolic III
1450988_at	Lgr5	0.000104528	-1.128020167	leucine rich repeat containing G protein coupled receptor 5
1460259_s_at	Clca1 /// Clca2	4.81E-05	-1.1227931	chloride channel calcium activated 1 /// chloride channel calcium activated 2
1425140_at	Lactb2	6.22E-05	-1.1223803	lactamase, beta 2
1423155_at	Sri	2.21E-05	-1.116169533	sorcin
1429352_at	Mocos	0.001832595	-1.1025282	molybdenum cofactor sulfurase
1449071_at	Myl7	5.08E-05	-1.100698967	myosin, light polypeptide 7, regulatory
1451461_a_at	Aldoc	0.000126875	-1.096107167	aldolase 3, C isoform
1416842_at	Gstm5	6.66E-05	-1.0933743	glutathione S-transferase, mu 5
1436996_x_at	Lzp-s	3.63E-05	-1.0849762	P lysozyme structural
1417430_at	Cdr2	4.61E-06	-1.080600767	cerebellar degeneration-related 2
1449122_at	3110003A22Rik	0.001243961	-1.0788229	RIKEN cDNA 3110003A22 gene
1416152_a_at	Sfrs3	0.001468163	-1.074717033	splicing factor, arginine/serine-rich 3 (SRp20)
1451787_at	Cyp2b10	0.000117668	-1.063870267	cytochrome P450, family 2, subfamily b, polypeptide 10
1448813_at	Aadac	0.000309393	-1.062162967	arylacetamide deacetylase (esterase)
1421936_at	Dapp1	0.001381256	-1.043207967	dual adaptor for phosphotyrosine and 3-phosphoinositides 1
1419552_at	Echdc1	1.18E-06	-1.034101833	enoyl Coenzyme A hydratase domain containing 1
1422645_at	Hfe	0.001255647	-1.0315953	hemochromatosis
1423569_at	Gatm	0.000753683	-1.025528	glycine amidinotransferase (L-arginine:glycine amidinotransferase)
1428113_at	4930403J22Rik	0.000133631	-1.0226883	RIKEN cDNA 4930403J22 gene
1450825_at	Asah3	0.00011572	-1.015298967	N-acylsphingosine amidohydrolase (alkaline ceramidase) 3
1448050_s_at	Map4k4	3.39E-07	1.00211	mitogen-activated protein kinase kinase kinase kinase 4
1425895_a_at	Id1	0.000735193	1.010493633	inhibitor of DNA binding 1
1439389_s_at	Myadm	0.00207017	1.0136956	myeloid-associated differentiation marker
1434514_at	Rbm15	0.000111617	1.017873833	RNA binding motif protein 15
1416067_at	Ifrd1	1.41E-05	1.021099567	interferon-related developmental regulator 1
1451776_s_at	MGI:1916782	0.001074486	1.023476767	homeobox only domain
1423271_at	Gjb2	9.08E-05	1.028331467	gap junction membrane channel protein beta 2
1427095_at	Cdcp1	7.87E-05	1.032642733	CUB domain containing protein 1
1449424_at	Plek2	5.27E-05	1.0355516	pleckstrin 2
1425606_at	Slc5a8	2.62E-05	1.037546	solute carrier family 5 (iodide transporter), member 8
1416762_at	S100a10	8.16E-06	1.0443273	S100 calcium binding protein A10 (calpactin)
1421262_at	Lipg	3.83E-05	1.052711133	lipase, endothelial
1421997_s_at	Itga3	2.82E-05	1.061272467	integrin alpha 3
1417328_at	Ercc1	2.06E-05	1.0757111	excision repair cross-complementing rodent repair deficiency, complementation group 1
1419498_at	2010002A20Rik	1.98E-05	1.088392667	RIKEN cDNA 2010002A20 gene
1438019_at	1810043M15Rik	1.19E-05	1.097905033	RIKEN cDNA 1810043M15 gene
1433733_a_at	Cry1	3.48E-05	1.108288333	cryptochrome 1 (photolyase-like)
1418970_a_at	Bcl10	5.42E-05	1.129694433	B-cell leukemia/lymphoma 10
1455158_at	Itga3	0.000114722	1.1318796	integrin alpha 3
1436584_at	Spry2	3.03E-05	1.159752133	sprouty homolog 2 (Drosophila)
1435226_at	Ibrdc3	4.25E-06	1.1651381	IBR domain containing 3
1448612_at	Sfn	1.52E-05	1.1853238	stratifin
1448170_at	Siah2	7.78E-05	1.189715067	seven in absentia 2
1451680_at	Srxn1	5.95E-05	1.190804	sulfiredoxin 1 homolog (S. cerevisiae)
1454736_at	4921515A04Rik	0.000257945	1.2037354	RIKEN cDNA 4921515A04 gene
1419491_at	Defb1	8.38E-05	1.2146904	defensin beta 1
1442026_at	---	0.001730814	1.218938733	---
1422659_at	Camk2d	1.17E-05	1.225341733	calcium/calmodulin-dependent protein kinase II, delta
1427416_x_at	Dusp7	8.11E-07	1.239468533	dual specificity phosphatase 7
1424711_at	Tmem2	3.20E-06	1.253082733	transmembrane protein 2
1416871_at	Adam8	4.01E-05	1.2798786	a disintegrin and metallopeptidase domain 8
1423321_at	Myadm	0.00039799	1.281268567	myeloid-associated differentiation marker
1432478_a_at	Ibrdc3	5.46E-05	1.286755033	IBR domain containing 3
1451375_at	Ehf	0.006790813	1.314848633	ets homologous factor
1449852_a_at	Ehd4	4.06E-05	1.330769767	EH-domain containing 4
1420088_at	---	9.21E-05	1.3857817	---
1428081_at	Klhl21	0.000124064	1.389375067	kelch-like 21 (Drosophila)
1425351_at	Srxn1	0.000856198	1.397189133	sulfiredoxin 1 homolog (S. cerevisiae)
1425837_a_at	Ccrn4l	5.40E-05	1.420894167	CCR4 carbon catabolite repression 4-like (S. cerevisiae)
1424268_at	Smox	3.88E-06	1.421619	spermine oxidase
1451612_at	Mt1	0.000662259	1.433491867	metallothionein 1
1424040_at	Rprc1	2.96E-06	1.447909767	arginine/proline rich coiled-coil 1
1434369_a_at	Cryab	8.07E-05	1.474317467	crystallin, alpha B
1430125_s_at	Pqlc1	5.03E-06	1.5516156	PQ loop repeat containing 1
1424942_a_at	Myc	2.56E-05	1.576376833	myelocytomatosis oncogene
1450188_s_at	Lipg	2.70E-07	1.5773951	lipase, endothelial
1416442_at	Ier2	0.001166582	1.582609667	immediate early response 2
1423100_at	Fos	0.001007956	1.615779967	FBJ osteosarcoma oncogene
1417065_at	Egr1	3.16E-05	1.6236002	early growth response 1
1423233_at	Cebpd	0.000140625	1.6567732	CCAAT/enhancer binding protein (C/EBP), delta
1449731_s_at	---	1.96E-05	1.662402733	---
1426567_a_at	Pqlc1	8.53E-05	1.700366967	PQ loop repeat containing 1
1421943_at	Tgfa	1.12E-05	1.758150067	transforming growth factor alpha
1426875_s_at	Srxn1	6.67E-05	1.769540467	sulfiredoxin 1 homolog (S. cerevisiae)
1451594_s_at	Serpinb6c	4.47E-06	1.8033144	serine (or cysteine) peptidase inhibitor, clade B, member 6c
1431339_a_at	Efhd2	0.00012266	1.8041541	EF hand domain containing 2
1416431_at	Tubb6	0.000143601	1.8068879	tubulin, beta 6
1460393_a_at	Dusp7	0.000651256	1.810689633	dual specificity phosphatase 7
1448529_at	Thbd	0.00011617	1.8242792	thrombomodulin
1419474_a_at	Ehf	0.000180638	1.833449667	ets homologous factor
1422240_s_at	Sprr2h	3.50E-05	1.841429867	small proline-rich protein 2H
1448932_at	Krt1-16	1.34E-05	1.875484	keratin complex 1, acidic, gene 16
1423306_at	2010002N04Rik	1.99E-05	1.896356467	RIKEN cDNA 2010002N04 gene
1419492_s_at	Defb1	0.000619932	1.9224169	defensin beta 1
1431936_a_at	Neu2	7.90E-05	1.931981333	neuraminidase 2
1419431_at	Ereg	0.000117409	1.9552495	epiregulin
1452519_a_at	Zfp36	0.000775952	2.038867167	zinc finger protein 36
1448306_at	Nfkbia	1.12E-05	2.064505167	nuclear factor of kappa light chain gene enhancer in B-cells inhibitor, alpha
1424086_at	D9Ucla1	1.05E-05	2.127011067	DNA segment, Chr 9, University of California at Los Angeles 1
1452418_at	1200016E24Rik	7.02E-05	2.127970167	RIKEN cDNA 1200016E24 gene
1422704_at	Gyk	7.48E-07	2.242385433	glycerol kinase
1415834_at	Dusp6	4.53E-05	2.303629767	dual specificity phosphatase 6
1427005_at	Plk2	0.00015386	2.321262233	polo-like kinase 2 (Drosophila)
1453238_s_at	E430024C06Rik	6.46E-06	2.541364733	RIKEN cDNA E430024C06 gene
1418133_at	Bcl3	1.37E-06	2.631146867	B-cell leukemia/lymphoma 3
1455899_x_at	Socs3	0.001355354	2.667132867	suppressor of cytokine signaling 3
1418349_at	Hbegf	0.000360589	2.676067567	heparin-binding EGF-like growth factor
1423933_a_at	1600029D21Rik	0.000123509	2.697311233	RIKEN cDNA 1600029D21 gene
1449133_at	Sprr1a	2.86E-05	2.740214633	small proline-rich protein 1A
1422784_at	Krt2-6a	0.00956	2.959487775	keratin complex 2, basic, gene 6a
1435137_s_at	1200016E24Rik	5.00E-07	2.9949676	RIKEN cDNA 1200016E24 gene /// hypothetical gene supported by AK004796
1417487_at	Fosl1	0.000145519	3.147900067	fos-like antigen 1
1427932_s_at	1200003I10Rik	7.53E-08	3.3668875	RIKEN cDNA 1200003I10 gene /// hypothetical gene supported by AK004796
1427700_x_at	Krt2-6a	0.00233	3.368921485	keratin complex 2, basic, gene 6a
1449994_at	Epgn	6.69E-05	3.393066233	epithelial mitogen
1448377_at	Slpi	6.55E-05	3.704208267	secretory leukocyte peptidase inhibitor
1422783_a_at	Krt2-6a	0.00329	3.808532470	keratin complex 2, basic, gene 6a
1419209_at	Cxcl1	7.07E-05	3.834693967	chemokine (C-X-C motif) ligand 1
1421134_at	Areg	3.41E-05	3.8750889	amphiregulin
1448756_at	S100a9	2.28E-05	4.412246767	S100 calcium binding protein A9 (calgranulin B)
1419149_at	Serpine1	5.11E-05	4.503452567	serine (or cysteine) peptidase inhibitor, clade E, member 1
1421806_at	Defb3	0.001294852	4.6443679	defensin beta 3
1456001_at	Sprrl1	0.005068762	5.260587367	small proline rich-like 1
1422963_at	Sprr2i	3.74E-06	5.530648	small proline-rich protein 2I
1419394_s_at	S100a8	0.000404717	5.535525667	S100 calcium binding protein A8 (calgranulin A)
1450811_at	Sprr2j	1.96E-06	5.781713433	small proline-rich protein 2J
1449833_at	Sprr2f	2.57E-05	6.081538533	small proline-rich protein 2F

Supplementary Table S2. List of antibodies used.

Antigen	Antibody	Vendor/Catalog#	Dilution	Secondary antibody
Arnt	Goat polyclonal	Santa Cruz, CA/ sc-8076	1:150	Donkey anti-goat Ig G-B (sc-2042, Santa Cruz)
Filaggrin	Rabbit polyclonal	Covance Research Products, CA/ PRB-417P	1:500	Goat anti-rabbit Ig G-B (sc-2040, Santa Cruz)
Loricrin	Rabbit polyclonal	Covance Research Products, CA/ PRB-145P	1:200	Goat anti-rabbit Ig G-B (sc-2040, Santa Cruz)
Involucrin	Rabbit polyclonal	Covance Research Products, CA/ PRB-140C	1:500	Goat anti-rabbit Ig G-B (sc-2040, Santa Cruz)
b-actin	Rabbit affinity isolated antibody	Sigma-Aldrich/ A-2066	1:200	HRP-goat anti-rabbit IgG (H+L) (111-035-144, Jackson ImmunoResearch Lab)

Supplementary Table S3. Primers used for real-time PCR analysis

Sequence ID	Primer name	Sequence	Product length
AF347023	Asah3 S	5'-TGAGGTGGATTGGTGTGAGAG-3'	137
	Asah3 A	5'-TACGCTTCTGGGCATACGG-3'	
U73004	Slpi S	5'-TGTTCCCATTCGCAAACCAGTG-3'	217
	Slpi A	5'-GCACACCGAGCACGAGTCC-3'	
NM_013650	S100a8 S	5'-TCAAGACATCGTTTGAAAGGAAATC-3'	84
	S100a8 A	5'-GGTAGACATCAATGAGGTTGCTC-3'	
NM_009114	S100a9 S	5'-AAAGGCTGTGGGAAGTAATTAAGAG-3'	81
	S100a9 A	5'-GCCATTGAGTAAGCCATTCCC-3'	
M16465	S100a10 S	5'-GACCACTTGACAAAGGAGGAC-3'	374
	S100a10 A	5'-TTCTCTCTCAGATTGTTGAATTGG-3'	
AK152473	Arnt S	5'-TTTATCCCTAGAGATGGGTACAGG-3'	134
	Arnt A	5'-CCACAGGCTGGACAGAAACC-3'	
M33960	Serpine1 S	5'-CGCCTCCTCATCCTGCCTAAG-3'	190
	Serpine1 A	5'-CTGTGCCGCTCTCGTTTACC-3'	
X91824	Sprr1a S	5'-AGAGCCATGCCTGAAGACCTG-3'	258
	Sprr1a A	5'-CATACACTTGTCTCACTCCTCACC-3'	
NM_011475	Sprr2i S	5'-CCTGAGCCTTGTCCTGAGTC-3'	246
	Sprr2i A	5'-ATGTAGAAGGAGGTGCTATGTGG-3'	
NM_008508	Lor S	5'-CCTGTGGGTTGTGGAAAGACC-3'	102
	Lor A	5'-AGAGCCTCCTCCAGATGAGC-3'	
NM_008412	Ivl S	5'-AGAACTGCATCTGGGTCAGC-3'	146
	Ivl A	5'-GCTTCTGCTTCTGTTTCTGTCC-3'	
AK144782	Sprr1a S	5'-AGAGCCATGCCTGAAGACC-3'	130
	Sprr1a A	5'-TTTTAGGTGGTGCAAGGAGAG-3'	
AK003391	Sprr2a S	5'-GAAGTGCCCTGAGCCTTGTC-3'	133
	Sprr2a A	5'-AGGTGGGCATTGCTCATAGC-3'	
NM_011475	Sprr2i S	5'-TCTCACATGCCTCCATAGC-3'	95
	Sprr2i A	5'-CATGTAGAAGGAGGTGCTATG-3'	
NM_011476	Sprr2j S	5'-TGTCTTACCAAGAGCAGCAGTG-3'	142
	Sprr2j A	5'-TGGCAGTGGATAGGACTCTGG-3'	
NM_033175	Sprrl1 S	5'-CTGCCAGCAGAGTCAGAAGC-3'	126
	Sprrl1 A	5'-CTTGTAGCACAGCAGGAAGAGG-3'	
X03672	Actb S	5'-CCTTCTTGGGTATGGAATCCTGTG-3'	98
	Actb A	5'-TGTGTTGGCATAGAGGTCTTTACG-3'	